

University of Pannonia
Department of Electrical Engineering and Information Systems
Doctoral School of Information Science



OPTIMAL CURRENT CONTROL FOR DOMESTIC POWER CONVERTERS

DOI:.....

Doctoral (PhD) Thesis
Author: László Richard Neukirchner

Supervisor: dr. Magyar Attila

Made at University of Pannonia Doctoral School of Information Science

Veszprém
2019

OPTIMAL CURRENT CONTROL FOR DOMESTIC POWER CONVERTERS

Értekezés doktori (PhD) fokozat elnyerése érdekében

Írta:

László Richard Neukirchner

Készült a University of Pannonia Doctoral School of Information
Science keretében

Témavezető: dr. Magyar Attila

Elfogadásra javaslom: igen / nem

.....
aláírás

A jelölt a doktori szigorlaton %-ot ért el.

Az értekezést bírálóként elfogadásra javaslom:

Bíráló neve: : igen / nem

.....
aláírás

Bíráló neve: : igen / nem

.....
aláírás

A jelölt az értekezés nyilvános vitáján %-ot ért el.

Veszprém,

.....
a Bíráló Bizottság elnöke

A doktori (PhD) oklevél minősítése:

.....
az EDHT elnöke

Acknowledgement

I wish everybody the best!

Abstract

Voltage unbalance is a major yet often overlooked power quality problem in low voltage residential feeders due to the random location and rating of single-phase renewable sources and uneven distribution of household loads. This paper proposes a new indicator of voltage **deviation** that may serve as a basis of analysis and compensation methods in this dimension of power quality. The paper proposes three main results. First of all a novel voltage norm capable of indicating unbalance and **under-voltage in a single value**. Afterwards, a three phase unbalance reduction controller structure is given. As the third main result, the proposed controller structure is integrated with an optimization based control algorithm that uses asynchronous parallel pattern search as its engine. The suggested structure and the underlying three phase power grid model has been implemented in a dynamical simulation environment and tested against engineering expectations. The simulation based experiments served as a proof of concept for the proposed complex control structure. The experiments included performance and robustness analysis, both of them concluded that the proposed control and inverter structure is promising. The proposed three phase inverter structure together with the control algorithm connected with a renewable source (photovoltaic panel or wind turbine) is capable of an asymmetric power injection **or rerouting the energy flow** to the grid so that the voltage unbalance decrease. This is also important from the environmental point of view since the achieved power loss reduction can easily be translated to CO₂ emission reduction and carbon footprint - these indicators has also been calculated.===

This Thesis is consisted about optimal control of power converters. The first part is consisting of a constrained optimal control of a current source rectifier (CSR) is presented, based on a mathematical model developed in Park's frame. To comply with the system constraints an explicit model-based predictive controller was established. To simplify the control design, a disjointed model was utilised due to the significant time constant differences between the AC and DC side dynamics. As a result, active damping was used on the AC side, and explicit Model Predictive Control (MPC) on the DC side. The results are compared by simulation with the performance of a state feedback control. This is followed by developing a cost function for mitigating voltage asymmetry on a domestic network, which requires only measuring the voltage whilst only current interventions are required. Lastly an asymmetric inverter structure was developed to serve the cost function minimizing compensational needs. Results were implemented and validated with Matlab simulations.

List of contents

1	Introduction	1
1.1	Literature overview	3
2	Basic notions	8
2.1	Definitions of voltage unbalance	8
2.1.1	Types of voltage deviations and norms	8
2.1.2	Non standardized approximations formulas	9
2.1.3	LVUR	10
2.1.4	PVUR	10
2.1.5	VUF and CVUF	11
2.2	Current source inverters	12
2.3	Galvanic decoupled bi-directional DC-DC converters	14
2.4	Three-phase buck-type rectifiers	15
2.4.1	Basic operation principles	17
2.5	Asynchronous parallell pattern search	19
2.5.1	Parallel pattern search	19
2.5.2	Adding asynchronity	19
2.6	Quadratic optimization and model predictive control (MPC)	20
2.6.1	Overview on predictive control	21
2.6.2	Constained optimal control	21
2.6.3	Stability of MPC	24
2.7	Explicit model predictive control (EMPC)	27
2.7.1	Storage of critical regions	28
3	Voltage unbalance compensation	30
3.1	Network structure	30
3.2	Proposed geometrical indicator	31
3.3	The method's additional content compared to VUF	32
3.4	Unbalance compensation	36
3.4.1	Problem statement	36
3.4.2	Control problem	37
3.4.3	Optimization based control algorithm	40
3.5	Discussion	42
3.5.1	Dynamical simulation based experiments	42
3.5.2	Performance analysis	42
3.5.3	Environmental effect	44

3.6	Conclusion	46
4	Predictive control of a CSR	48
4.1	Modeling	48
4.1.1	Mathematical Modeling of the CSR	48
4.1.2	Model simplification	50
4.1.3	Control structure	51
4.2	Control	52
4.2.1	DC-side explicit model predictive control	52
4.2.2	Active AC-side damping	55
4.3	Space vector modulation strategy	56
4.4	Modulation	56
4.5	Discussion	59
4.5.1	Computational effort	59
4.5.2	Horizon performance	59
4.5.3	Simulation results	60
4.5.4	Comparison with a state feedback control	61
4.6	Conclusion	62
5	Summary	64
5.1	Thesis: Constrained, explicit predictive control for current source buck-type rectifiers	64
5.2	Thesis: Geometrical indicator for voltage unbalance in three phase networks	64
5.3	Thesis: Voltage unbalance compensation with optimization based control algorithm and asymmetrical inverter structure	65

Chapter 1

Introduction

Growth of distributed generation from renewable energy sources and the nature of the electrical power grid initiated a trend to alter from a passive network to an active one. So called smart grids have the ability to provide much more in depth observable measurement results of they customers, grid operators and energy traders alike. Through voltage and current measurements, the habits of each actor (household, station, or industrial- commercial facility) can be easily mapped and taken into account. Moreover, the potential failure could be indicated and preemptively acted upon, before irreversible malfunction, significant amount of wear, or generally, the efficiency of energy consuming actor's power electric consumer's diminishes. In most cases, only smart metering is present, whilst central control and measurement is not an option.

In this new environment, the importance and difficulty of maintaining and operational stability and cost effective control of the distribution system are increasing together. With this in mind local solutions are the most convenient solutions, and as opposed to this expectation most of a household's possible renewable sources and loads are unevenly distributed, without mindful control over single phase power converters. Some of these could represent an unevenly high power consumption, or worse a locally significant energy source in times where it's most unnecessary, especially outside peak zones of consumption. The situation is further exacerbated by the stochastic on/off switching of the different types of loads which causes stochastic disturbing unbalance in the load currents which cases unbalanced load of the low voltage transformer, and causes amplitude and phase unbalance in the voltage phasor trough the serial impedance of the low voltage transportation line wires and connecting devices cables.

If we observe the opposite side, ideal generators supply symmetrical three-phase sinusoidal (mostly only) positive sequence voltages, which are balanced in terms of their amplitudes phase differences at a single frequency. With this in mind, without taking the said gap, voltage (as such consumption- and production-) unbalance occurs on the network. The terminology of unbalance can be divided into amplitude unbalance, phase difference unbalance, and unbalanced harmonic disturbance. The occurrence of at least one of these

features is enough for a distribution network to become unbalanced.

Many countries have changed their regulating laws about power supply to allow for grid-tie inverter systems to provide spare power from renewable sources to local low voltage grids. The unbalance of the grid is further increased by using single phase grid tie inverter systems in the size of typical small household power plants (1 - 50 kW) and the produced electrical power originating from renewable power source (wind and solar) also admits stochastic behavior. This unbalance yields to a suboptimal operation of low voltage three phase transformers and machines to generate undesirable additional yield loss and increase in the probability of malfunction of the low voltage energy transportation system's components, or the effective current unbalance could cause additional power loss of the transportation line resistances or in the end complete shut-down.

To mitigate or avoid such situations an approach is required, where the system where said phenomena occurs is an optimization problem. However to formulate an optimization problem, many things should be layd down to formulate it properly. Most importantly, a cost function should be established which can bi served as a local (or global minima) for solving the question. For instance, if voltage unbalance would be eliminated, than the correct indicator of unbalance should serve as basis, moreover the deviation from the optimum could be quadratic.

Such tasks can not be achieved without proper instrumentation. To be able to apply control, where he voltage levels are designated, and the end user has no direct control (only the plant or transformer level has such), deviations can be addressed, and current control can be used as actuation. This way a control structure can be imagined for a power electric converter, where every step should cont towards the optimum state, with respect of the energy (or control reserves), wear of the device (sub components, namely gates have finite switching capabilities), and safety constraints (designated level of current and voltage should not trespass a given hard constraint for the sake of malfunction avoidance, and soft constraint for the sake of reducing wear). Additionally it should not be forgotten, that with all the above, the device should operate in the domains of kHz or above, and it shoud be run on a cheap device, like an embedded micro-controller chip or DSP. With all this in mind an the designed power electric structure can be designed to fulfill the high standers of today's requirements. The problem is, conventional controllers can not achieve this all at once. The methodology based on optimal control, was originally designed for highly complex, and safety critical systems, with huge amount of inputs and outputs, power plants, and chemical- or refinery plants. This system though have an incomparably lower time constant, which renders conventional model based predictive controllers useless in the domain of power electronics.

To marry the two approaches together, a solution came up from the automotive industry. A car is also a highly safety critical multiple-input, multiple-output (MIMO) system with obvious constraints, in increasingly changing environment. The key is, to map said environment and in it every state, the system can, or allowed to achieve. Where constraints are present, finite states can be

defined, either by hand (e.g. statemachines) or by advanced mapping algorithms, and then in every little kingdom, a relatively simple (linear if possible) rule where one state of the system dynamics could be substituted, then to make sure stepping on to the next most applicable rule can be achieved very fast. This way, by choosing the resolution of the mapping correctly (too fine resolution gives too high processing requirements, too low gives suboptimal dynamics), the predictive control approach can be applied in both worlds. In this thesis..

1.1 Literature overview

Single phase power injections to the grid are mainly generated by domestic photovoltaic-(PV) and wind power plants. Many current references about the renewable energy sources integration to the low voltage grid are short-, and long-time storage ready for connection of this electrical energy in the literature can be found. For off-grid, sometimes more complex solutions integrating diesel generators, PV and wind generators. Such as proposed, in [79]. [20] where presented the economical aspects of a PV system. The economic results are strongly influenced by the annual average isolation value, which encourages the areas most exposed to the sun and the southern areas. The consumption of consumers is not critically important, but the design principle used has as significant effect on the maximization of the performance of PV plants. In [42] worth noticing, that autonomous photovoltaic systems are strongly responsible of their reactive energy requirements. To support photovoltaic systems with battery banks sustainable character one should be able to establish that their reactive energy requirement share fairly compensated by the corresponding energy yield. Additionally, in [65] the author emphasizes that PV systems are increasingly being deployed in all over the world, and this is the source of a wide range of power quality problems. With a view to consistently measuring and assessing the power quality characteristics of PV systems, they had presented an in-depth overview and discussion of this topic.

The study by [77] explored integration issues of electric vehicle battery packs. They suggest that high voltage battery packs with large format cells has advantages in assembly, thermal management, monitoring and control, services and maintenance. On the other hand, quality, reliability and limited specific energy of large format cells are obstacles need to overcome. Solving these problems will further affect the cost, performance, reliability and safety of the electric vehicles. Smart energy systems in specially in urban areas are discussed in [53] where a design methodology has been suggested.

Many power systems, voltage parameters change over time. Variation of power quality disturbances leads to thermal transients in electrical machines. This problem can be especially important in the case of low-power machines, because they have shorter time constants than high-power ones. The rate of thermal responses of a machine also significantly depends on the type of power

quality disturbances. Voltage unbalance can cause machine overheating within a mere few minutes. Furthermore, fluctuating unbalance could cause an extraordinary rise in windings temperature and additional thermo-mechanical stress. Consequently, voltage unbalance is found to be more harmful to induction motors than the results from previous works [28]. Additionally beside the heat factor, voltage unbalance can cause increased reactive power [76], various copper loss [80] torque pulsation in electric motors [15] have been studied. [50] were discussing the effects of unbalanced voltage on a three-phase induction motor, one has to consider not only negative-sequence voltage but also the positive-sequence voltage. With the same voltage unbalance factor, the status of voltage unbalance could be judged by the magnitude of positive sequence voltage. Also the effect of voltage unbalance has been studied on three-phase four-wire distribution networks for different control strategies for three-phase inverter-connected distributed generation units on voltage unbalance in distribution networks ([56]). Here the negative-sequence component and the zero sequence component were studied where unbalance conditions could lower stability margin and increasing the power losses. On the other hand, the adaptive coordination of distribution systems included distributed generation is also an emerging problem as it was discussed by [8]. A small voltage unbalance might lead to a significant current unbalance because of low negative sequence impedance as highlighted in [12].

As such at the University of Pannonia a previous work of [31] a complex control unit has been proposed that is capable of lowering extant harmonic distortion. In the work of [30] the effect of a small domestic (photovoltaic) power plant on the power quality, mainly the total harmonic distortion has been examined. The aim of this work is to examine and compensate three phase voltage asymmetry of the electrical network based on the extended simulation model proposed by [31]. Further control methods were applied for the solution for balancing of the most sensitive with regard to electric energy quality part of power system in [48], minimizing the active power losses, stabilization of three-phase voltages, enhancement of asynchronous machine performance stability and reduction of errors occurring in power consumption measuring circuits.

In many articles the authors presents a different viewpoint of calculating unbalance on the network. [55] showed to assess the harmonic distortion and the unbalance introduced by the different loads connected to the same point of common coupling have been applied to an experimental distribution network. By [45] the focus was to bring out the ambiguity that crops up when we refer to a particular value of voltage unbalance that exists in the system. By making use of the complex nature of voltage unbalance, the voltage combinations that lead to the calculation of complex voltage unbalance factor could be narrowed down to a great extent. A fast and accurate algorithm for calculating unbalance has been presented by [94]. The magnitudes of zero, positive, and negative sequences are obtained through simple algebraic equations based on

the geometric figure, which is also called as 4 and 8 geometric partitions. Also a three-phase optimal power flow calculation methodology has been presented by [6], that is suitable for unbalanced power systems. The optimal algorithm uses the primal-dual interior point method as an optimization tool in association with the three-phase current injection method in rectangular coordinates.

There are different approaches of lowering the unbalance with different control techniques. Additionally, new computationally efficient control techniques have been presented by [51] to estimate and compensate input voltage-unbalance disturbances for a voltage source converter. These tools are designed to be effective with high power systems with slower PWM switching frequencies of 5 kHz or lower and limited current-controller bandwidth. About the unbalance compensation control aspect, a three-phase IGBT-based static synchronous compensator were proposed for voltage and/or current unbalance compensation by [95]. An instantaneous power theory was used for real-time calculation and control. Three control schemes current control, voltage control and integrated control were proposed to compensate unbalanced voltage, unbalanced current or both. Unbalance phenomena and power quality can be examined with modeling too. A particular modeling method was presented by [52], where a three-phase four-wire grid-interfacing power quality compensator were modeled. During grid voltage unbalance, the compensator, used a shunt and a series four phase inverter, and could enhance both the quality of power within the microgrid and the quality of currents flowing between the microgrid and utility system, where a microgrid is a group of interconnected loads and distributed energy resources within clearly defined electrical boundaries that acts as a single controllable entity with respect to the grid. A microgrid can connect and disconnect from the grid to enable it to operate in both grid-connected or island-mode. The shunt four-leg inverter were controlled to maintain a set of balanced distortion free voltages to regulate power sharing among the parallel-connected distributed generation systems. Simulation studies were carried out by [39] where one of the aims was to develop and test the feasibility of a decoupled three-phase on-load tap charger in the distribution system with the objective of improving the distribution network power quality. Further control methods were applied for the solution for balancing of the most sensitive with regard to electric energy quality part of power system by [48], minimizing the active power losses, stabilization of three-phase voltages, enhancement of asynchronous machine performance stability and reduction of errors occurring in power consumption measuring circuits.

In the arsenal of voltage unbalance compensation, current source power electronic devices have a dedicated position. Based on the instantaneous active power theory under unbalanced grid conditions [93] proposes an optimized negative-sequence current references for eliminating the double-frequency oscillations on active power at AC side of a current source converter. The author argues in [90] that a classification of the virtual impedances can greatly benefit an unbalance compensating control structure, with an active stabilization

method. In [32] direct control strategy with detailed current converter model is shown which is much simpler than the complicated instantaneous power theory approach. This solution needs less voltage and current sensors for the feedback control, which means that it is a cost-effective solution. An interesting, yet similar approach compared in the paper is a bi-directional current source topology is used like in [87]. This enables to compensate a much larger degree of freedom handling unbalanced conditions with the precaution of unstable operation possibilities.

Current source rectifiers (CSR) are widely used in front-end power electronic converter for the uncontrollable or controllable DC-bus in industrial and commercial applications. They have maintained their position through many applications, with uses such as medium-voltage high-power drives [86], [27] STATCOMs [33] and renewable systems [18], [23]. They have a plain and reliable circuit structure, which makes them attractive for simple control design. The CSRs are traditionally controlled by state feedback, or classic cascaded linear control loops such as PI controllers. These simple control applications are suitable for induction motor control [17], and other electromechanical actuators [73], and unusual topologies [61]. Also, worth mentioning of self-tuning variants of PI controllers [83].

In the past, the modulation methods used were trapezoidal pulse width modulation techniques (TPWM), or application of pulse patterns calculated offline for selective harmonic elimination (SHE). More recently, current space vector modulation (SVM) has been used for the synthesis of the transistor control signals [26]. Even so, AC-side harmonic elimination could still be an issue at lower switching frequencies where LCL filtering (inductive-capacitive-inductive) would be advised [35].

In order to keep switching frequencies low and to minimize switching losses, new topologies and hybrid modulations are used, mixing TPWM and SHE depending on the grid frequency [88].

In terms of the amplitude of the grid and DC-link voltages, CSRs exhibit a step-down conversion. When used as DC voltage source, the rectifier can output a lower DC voltage without the need of a grid-side transformer, as is usually employed in voltage source rectifiers (VSR). Because of their current source behavior, CSRs can be easily paralleled and provide inherent short-circuit protection, representing an excellent potential in DC power supply applications [24], [96].

There are several control strategies in addition to classical PI control for applications in this domain. Self-adapting control methods are on the rise with more sophisticated algorithms in the field of fuzzy logic [85]. They are capable of handling increasingly more complicated models and systems with high dynamics and accuracy [16], [34], and even without establishing and validating

classical state-space models [89]. The other field is the sliding mode control, which can achieve good dynamic performance and handle non-linearity. Still, they might also introduce chattering, which can be very undesirable when applied to real-life systems like in [69] and [82]. Additionally in [5] the validity of an MPC-based, digital pulse width modulation control strategy for single-phase voltage source rectifiers is discussed, further confirming the validity of this method in control systems.

In the linear domain implicit model predictive control (IMPC or just MPC) is a fair solution due its effectiveness in power electronics due to its configurable cost function and such scalable nature [43], [5]. In this field also finite-state solutions are present which can be considered also predictive control, where the modulation scheme's defined states serve as optimization potential [70], [29]. As a further step adaptive application was established to tackle parameter estimation problems for better performance [58]

Recently, beside implicit, finite-state, and adaptive predictive control, explicit model predictive control has emerged in the field of power electronics [49]. Establishing the MPC cost function can range widely depending on the expected dynamics, degree of noise cancellation, and model complexity. Additionally, the current limitation can also be implemented introducing constraints in the modulation algorithm.

Chapter 2

Basic notions

In this chapter the basic topics of the thesis are discussed. First the phenomena of voltage unbalance on small distribution networks are shown and the ambiguities through the development of the concept, and at the end the norm currently in use in the industry. Next a necessary glimpse of power electric background is given to invite to the viewpoint of the modeling and problem breakdown of power converter. Lastly the basis of model based predictive methodology shall be shown, with the end with the explicit partition of the state space for a computationally efficient approach.

2.1 Definitions of voltage unbalance

Voltage unbalance is such a phenomena where the three phase voltages differ in amplitude normal 120 degree phase relationship. In most cases both are happening at the same time. This includes unequal voltage magnitudes at the fundamental frequency, either under, or over voltage, at the fundamental phase angle deviation. This is observed as a frequently cited power quality issue in low-voltage domestic distribution networks and in systems that supply large single phase loads unevenly distributed. Effects of voltage unbalance are complex, but can be categorized as structural or functional. The former refers to the asymmetry in the three-phase impedances of transmission lines, cables, transformers, etc. It occurs because it is neither economical nor necessary to maintain distribution system with perfectly symmetrical impedances. The latter refers to uneven distribution of power consumption over the three phases. Although the term voltage unbalance is unambiguous, the root phenomenon may be various as well as the standard norms used to measure unbalance. All of these different indicators measure voltage unbalance but each of them does it in a different way (??). In this section a detailed explanation is presented about the types of currently used method for indication.

2.1.1 Types of voltage deviations and norms

Voltage unbalance is not a straightforward term. To understand the concept, unbalance is when on a given frequency (mostly fundamental frequency)

voltage vectors (phase or line depending on the definition) deviating from the ideal in terms of length or angle. The first fall in to the category of unbalance, namely any kind of phase deviations, and unbalanced amplitude deviations, and balanced amplitude deviations, like under-voltage. There are many different technological causes with more or less practical importance. The following conditions are examined and tested in the sequel:

Single phase under-voltage unbalance If there is a single phase uncompensated overload in the system, the voltage in the overloaded phase will be lower than the other two.

Two phase under-voltage unbalance Two of the three phases are overloaded without compensation, the two overloaded phases will have higher voltage drop than the third phase. Balanced three phase under-voltage] The loads of all three phases are overloaded in an unbalanced manner.

Unbalanced single phase angle If the three phase voltage amplitudes are balanced but the relative angles between them (ideally it should be equal to ± 120 degree). It is assumed, that phase A would be the reference. If one of the other two phase angles is deflected, unequal displacement.

Unbalanced two phase angles displacement Similar to the single phase angle unbalance, if the other two phase angles are both deflected, then unequal angle displacement in two phase angles occurs.

An indicator of the voltage unbalance is supposed to measure the extent of unbalance but it is not expected to classify between the above types.

2.1.2 Non standardized approximations formulas

Up to now, the following definitions have not been adopted by any standard or rule to indicate the degree of voltage unbalance, but used by various manufacturers. Firstly based on [22] recommended by the CIGRE (International Council on Large Electric Systems, in french: Conseil International des Grands Réseaux Électriques), the voltage unbalance is determined with the following 2.1:

$$\begin{aligned} VUFactor &= \frac{\sqrt{1-\sqrt{3-6v}}}{1+\sqrt{3-6v}} \\ \text{where,} & \\ v &= \frac{V_{ab}^4 + V_{bc}^4 + V_{ca}^4}{(V_{ab}^2 + V_{bc}^2 + V_{ca}^2)^2}, \end{aligned} \quad (2.1)$$

where, $\{V_{ab}, V_{bc}, V_{ca}\}$ are the line-to-line voltages. Note, that the CIRGE variant has no distinct notation, as such it would be indicated as $VUFactor$ in this thesis. Moreover, the autor of [71] recommends two more variants, based on manufacturer recommended "standards":

$$VU = \frac{82 \cdot \sqrt{(V_{ab} - V_{avgline})^2 + (V_{bc} - V_{avgline})^2 + (V_{ca} - V_{avgline})^2}}{V_{avgline}} \times 100 \quad (2.2)$$

$$VUR = \frac{\max(|V_{ab}-V_{bc}|, |V_{bc}-V_{ca}|, |V_{ca}-V_{ab}|)}{V_{avgline}} \times 100, \quad (2.3)$$

where the line voltage mean is noted by and $V_{avgline} = \frac{V_{ab}+V_{bc}+V_{ca}}{3}$. This formulas were created with the intention to avoid the use of the complex algebra in symmetrical components and give a good approximation of the later described *VUF* standard. With the indicator of 2.2, and as well as 2.3. It is worth noticing, that only the voltage magnitude unbalance is reflected, completely ignoring Fortescue's method of symmetrical components [25] (shall presented later in the thesis), which considers negative sequence components as harmful on electric equipment and yield. Later we shall see that other methods try to push the same methodology, until the currently used norm (*VUF*) is used.

2.1.3 LVUR

One of the first voltage unbalance in percent is defined by the National Electrical Manufacturers Association (NEMA) [13] is defined as the ratio of the maximum voltage deviation from the average line voltage magnitude to the average line-voltage magnitude.

$$LVUR = \frac{\max(|V_{ab}-V_{avgline}|, |V_{bc}-V_{avgline}|, |V_{ca}-V_{avgline}|)}{V_{avgline}} \times 100 \quad (2.4)$$

The LVUR assumes that the average voltage is always equal to the rated value, which is 480 volts for the US three-phase systems, and it works only with magnitudes. Phase angles are not considered in this definition.

2.1.4 PVUR

The next phase voltage unbalance in percent described in IEEE standard 141. [1] (derived from [3]), is $PVUR_{IEEE-141}$. It is defined as the ratio of the maximum voltage deviation of phase voltages from the average phase-voltage magnitude to the average phase voltage magnitude. In various fields, LVUR and $PVUR_{IEEE-141}$ are commonly used to estimate the degree of voltage unbalance due to simplicity of calculation. The two unbalance factors mentioned above cannot completely reflect system voltage unbalance effects, such as the phase displacements of unbalanced voltages.

$$PVUR_{IEEE-141} = \frac{\max(|V_a-V_{avgphase}|, |V_b-V_{avgphase}|, |V_c-V_{avgphase}|)}{V_{avgphase}} \times 100, \quad (2.5)$$

where the voltages $\{V_a, V_b, V_c\}$ denotes the phase-to-neutral voltages, and $V_{avgphase} = \frac{V_a+V_b+V_c}{3}$. The second variant is, $PVUR_{IEEE-936}$, mentioned in [2] is defined as the ratio of the difference between the highest and the lowest phase-voltage magnitude to the average phase-voltage magnitude. Therefore, the numerical values of voltage balance quantified by $PVUR_{IEEE-936}$ are generally larger than those of $PVUR_{IEEE-141}$ and LVUR.

$$PVUR_{IEEE-936} = \frac{\max(|V_a|, |V_b|, |V_c|) - \min(|V_a|, |V_b|, |V_c|)}{V_{avg_{phase}}} \times 100, \quad (2.6)$$

The number of possible combinations of three phase or line voltages that satisfy the definitions of voltage unbalance mentioned above will become infinite as only the magnitudes of voltages are considered.

2.1.5 VUF and CVUF

The voltage unbalance factor (*VUF*) was defined by the International Electrotechnical Commission [68], [21]. From the theorem of symmetrical components [25], voltage unbalance can be considered as a phenomenon that positive sequence voltage (V_p) is disturbed by negative (V_n) and zero-sequence (V_0) voltages:

$$\begin{bmatrix} V_0 \\ V_p \\ V_n \end{bmatrix} = \frac{1}{3} \begin{bmatrix} 1 & 1 & 1 \\ 1 & a & a^2 \\ 1 & a^2 & a \end{bmatrix} \cdot \begin{bmatrix} V_a \\ V_b \\ V_c \end{bmatrix}, \quad (2.7)$$

Where $a = e^{2j\pi/3}$ is the Fortesque operator. From that the formulat of *VUF* can be formulated:

$$VUF = \left| \frac{V_n}{V_p} \right| \times 100, \quad (2.8)$$

This norm is currently in use world wide for voltage unbalance indication. The main focus in on the negative sequence compnent V_n , on which many studies attributes importance of the cause of negative effects the voltage unbalance causes.

As such, three-phase electric loads without path through the neutral, negative-sequence voltage is the primary cause of voltage unbalance. Normally, positive-sequence component of three-phase voltages is very close to rated value. If expressed in per-unit quantities, the positive-sequence voltage will be very close to 1.0 p.u., and the corresponding negative-sequence voltage will be very close to the *VUF*. Thus, the *VUF* can indeed be considered as the negative-sequence component in per-unit. This explains the advantage of using the *VUF* as an index for analyzing the effects of voltage unbalance considering the phase deviations. An extension of the *VUF* is the complex voltage unbalance factor (*CVUF*) that is defined by the ratio of the negative- sequence voltage phasor to the positive-sequence voltage phasor studied in [91], and [67]. The *CVUF* is a complex quantity having the magnitude and the angle. Although the *CVUF* has not yet been widely used by practicing engineers, it has been proposed in some studies (e.g., [92], [81], [19]) due to its richness of information on unbalance. The formula of *CVUF* is similar to *VUF*:

$$k_v = \frac{V_n}{V_p} = k_v \cdot e^{j\theta_v} = k_v \angle \theta_v, \quad (2.9)$$

where k_v is the magnitude and θ_v is the angle of *CVUF*.

It can be observed, that the previously mentioned norms of 2.1, 2.2, 2.3, 2.4, 2.5, 2.6, and 2.8 indicate different values for a single case with various correlations. The first two standard indicators, $PVUR_{IEEE-936}$ and $PVUR_{IEEE-141}$, ignore the ± 120 degree phase difference unbalance and only take the amplitudes into account. Additionally, the zero-sequence components never present in the line-to-line voltages regardless of the level of unbalance, only phase-to-neutral voltages. It has been proven, that these components are unelectable in some cases like bridge control of converters [11], or synchronous machine diagnosis [36].

The current state of the art definition in use, VUF , is sensitive to the phase difference unbalance. Lastly $CVUF$ considers also phase and magnitude of the voltage unbalance, but the two units are hard to merge together as the optimization cost of a cost function. Moreover, these definitions ignore zero sequence components and harmonic distortion that are always present in three-phase four-wire systems [12].

2.2 Current source inverters

Single-phase inverter's operating principles are different in each converter. The main features of the different approaches are reviewed and presented in the following. Although these converters cover the low-power range, they are widely used in power supplies or single-phase supplies. For this thesis a domestic current source inverter is considered, which fits into this category. A current source inverter is composed of capacitors, switches, and diodes, where an array of two switches is called inverter leg shown in Fig.2.1. The capacitors required to provide a neutral point, such that each capacitor maintains a constant voltage.

The inductors required are large, such that the inductors maintain a constant current i_i . Current-source topologies feature a low switching $\frac{dV}{dt}$ and reliable over-current or short-circuit protection. In order to operate properly the current-source inverter, we need to adhere to the following rules:

- Top or bottom switches of the different legs cannot be off simultaneously, because no current path is provided to the input inductors.
- Diode in series to each switch must be placed, because a short circuit across the output voltage V_o would be produced. If the commercial switch does not include anti-parallel diodes, then the circuit is already complete.
- In practical implementation, an overlapping time must be considered in the control signals of the top or bottom switches of the different legs.

According to the previous rules, it should be noticed that both switches of the inverter leg can be turned on at the same time, and this is not possible in voltage source inverters. There are four (1^{st} to 4^{th}) defined states of the switches and one not permitted switching state (5^{th} state) as shown in Table 2.1. The modulating technique should always ensure that at any instant, at

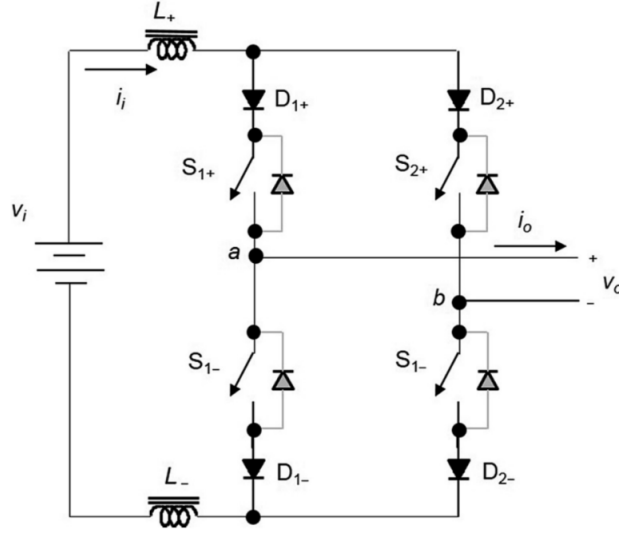


Figure 2.1: Topology of a singly phase current source inverter, where V_i , and V_o are the input and output voltages, i_i , and i_o are the input and output currents respectively. L_+ and L_- are current filter inductances, S_{1+} , S_{2+} , D_{1+} , and D_{2+} are the higher switches (controlled IGBTs for instance) and diodes, and S_{1-} , S_{2-} , D_{1-} , and D_{2-} are the lower switches and diodes respectively.

Components conducting				State	Output voltages		
S_{1+}	S_{2+}	S_{1-}	S_{2-}		V_{an}	V_{bn}	V_o
1	0	0	1	1	$V_i/2$	$-V_i/2$	V_i
0	1	1	0	2	$-V_i/2$	$V_i/2$	$-V_i$
1	1	0	0	3	$V_i/2$	$V_i/2$	0
0	0	1	1	4	$-V_i/2$	$-V_i/2$	0
0	-	0	-	5	Not permitted		
-	0	-	0				

Table 2.1: Switching states of the current source inverter, where V_{an} , V_{bn} are the a and b point's potential to ground.

least one of the top and bottom switch of the inverter legs is on, otherwise the inverter will be damaged.

The ideal waveforms are shown in Fig.2.2.

The states for the switches are defined by the modulating technique, which in this case is a carrier-based PWM, but unipolar output is considered. For the CSIs, different output filters may be employed, in order to provide the fundamental component of the output waveform. Depending on the application, it would be desirable to provide a voltage or current output.

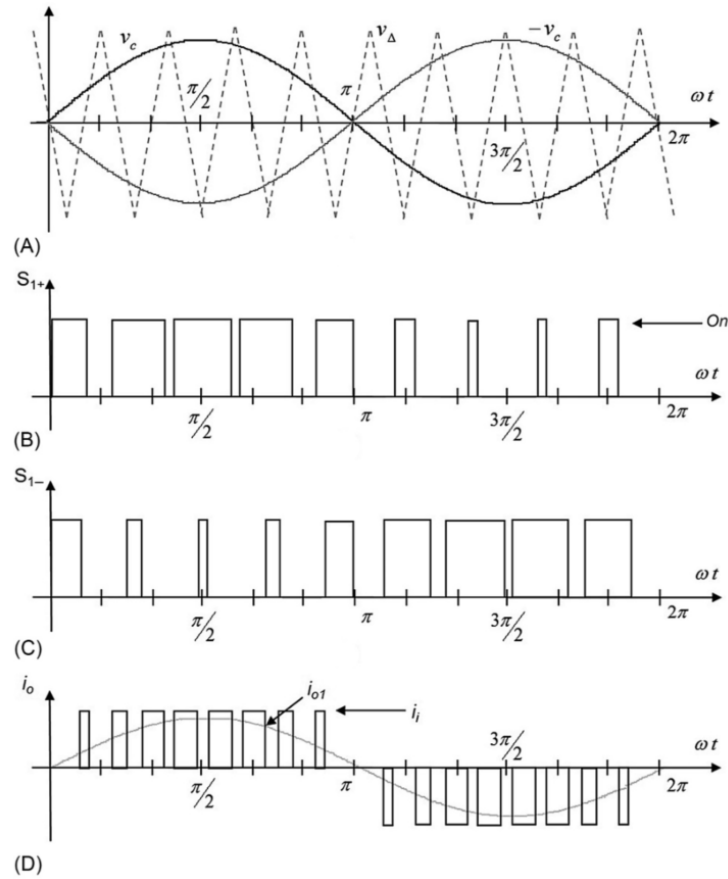


Figure 2.2: The CSI, ideal waveforms for the unipolar modulation: (A) carrier and modulating signals, (B) switch S_{1+} 's state, (C) switch S_{2+} 's state, and (D) AC output current.

2.3 Galvanic decoupled bi-directional DC-DC converters

In this section a basic galvanic decoupled voltage source DC-DC converter shall be presented. In many dc power supplies, a galvanic isolation between the dc or AC input and the DC output is required for safety and reliability. An economical mean of achieving such an isolation is to employ a transformer version of a dc-dc converter. High-frequency transformers are of a small size and weight and provide high efficiency. Their turns ratio can be used to additionally adjust the output voltage level. Generally, electric power generated by renewable energy sources is unstable in nature, thus producing a bad effect on the utility grid. This fact motivates research on energy storage and quality systems to smooth out active-power flow.

On Fig.2.3 the converter has two symmetrical single-phase voltage-source full-bridge converters, allowing a bi-directional power flow. Thanks to advancement in power device technology over the last decade has enabled the DC-DC devices to operate at an efficiency as high as $\approx 97\%$ by using the latest trench-gate IGBTs. Therefore this topology has become a promising candidate as a

power electronic interface for an energy storage and renewable system [44] [40].

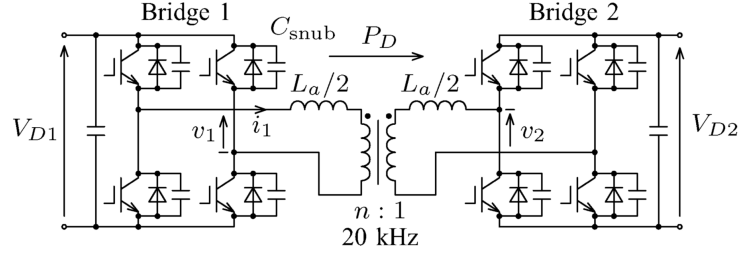


Figure 2.3: Bidirectional isolated dc-dc converter, where V_{D1} , and V_{D2} are the two end's voltage (in- and output depends on the power flow), v_1 and v_2 are the transformer voltages, C_{snub} are to reduce switching loss and to damp out over-voltage, and n is the transformer turn ratio.

The principle of operation of the DC-DC converter is very simple. Two active bridges are interfaced through a transformer and are phase shifted from each other to control the amount of power flow from one dc voltage source to the other. This allows a fixed frequency, square-wave mode of operation and utilization of the leakage inductance of the transformer as the main energy transfer element. The power transfer under idealized conditions is derived as:

$$P_D = \frac{V_{D1}V_{D2}}{\omega L} \left(\delta - \frac{\delta^2}{\pi} \right) \quad (2.10)$$

where $\omega = 2\pi f$ is the switching angular frequency of the two single phase full bridge controllers, L is the sum of the transformer leakage inductance.

2.4 Three-phase buck-type rectifiers

Three-phase controlled rectifiers have a wide range of applications, from small rectifiers to large high-voltage direct-current transmission systems. They are used for electrochemical processes, many kinds of motor drives, traction equipment, controlled power supplies, and many other applications. In this thesis only force commuted rectifiers are examined, which are built with semi-conductors (IGBTs in this case) with gate-turn-off capability. The gate-turn-off capability allows full control of the converter, because valves can be switched ON and OFF whenever is required. This allows the commutation of the valves, hundreds of times in one period that is not possible with line-commutated rectifiers, where IGBTs are switched ON and OFF only once a cycle. This has the following advantages:

- The current or voltage can be (pulse width) modulated, generating less harmonic contamination.
- The power factor can be controlled and even it can be made leading.
- They can be built as voltage-source or current-source based on the required application.

- The reversal of power in switching rectifiers is by reversal of voltage at the DC link. This allows force commutated rectifiers can be implemented for both, reversal of voltage or reversal of current.

There are two ways to implement force commutated three phase rectifiers (Fig.2.4), as a current-source rectifier, where power reversal is by dc voltage reversal, and as a voltage-source rectifier, where power reversal is by current reversal at the dc link.

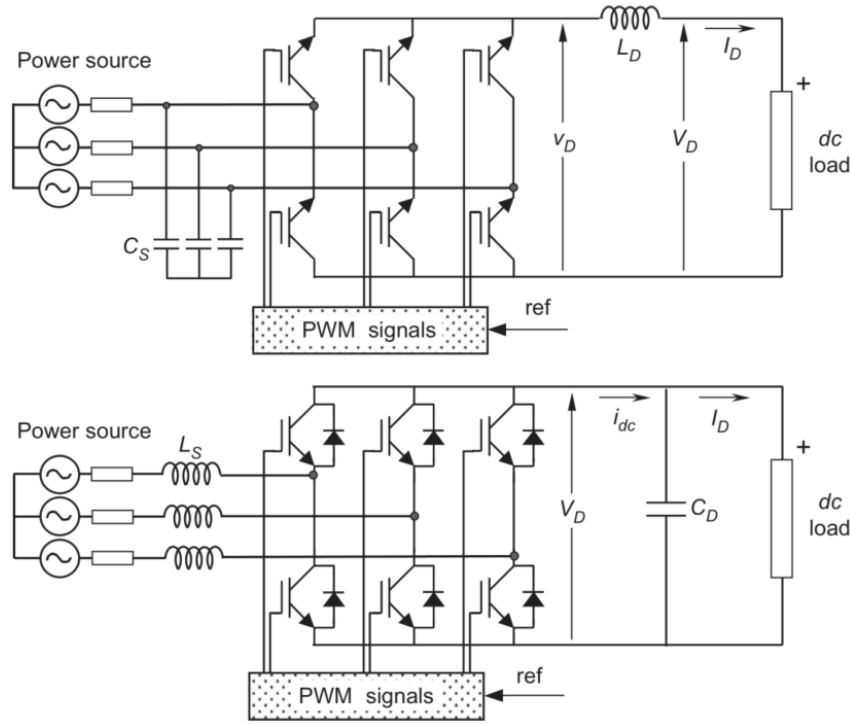


Figure 2.4: Basic topologies of force commutated rectifiers.

As general case a front-end converter power supply (e.g. lighting or telecommunications) shall be designed that should have approximately these general characteristics: sinusoidal main currents, unity power factor, high power density and simplicity of the power circuit structure. Two structures are most fitted for the task. First a boost-type input rectifier (e.g., Vienna rectifier, [46]), that typically features two 400V output voltages with a three-level isolated DC-DC converter or two isolated DC-DC output stage (see Fig. 4.1 in Ch.5.). The second candidate is the buck-type input rectifier (or current source rectifier (CSR)) (conventionally six-switch topologies as proposed in [97], [75]) with only one two-level isolated DC-DC converter output stage. Also the input stage can be realized as a three-switch topology with considerably lower system complexity as compared to the boost-type structure. In particular, the number of utilized active and passive components is much lower. Furthermore, there is no middle-point that has to be stabilized, as this is the case for the boost-type structures, making control and active filter design less complex. Further system advantages are the potential of direct start-up and

the implicit over current protection in case of an output short circuit. Therefore, this topologies of high interest for many safety critical applications as such future electric aircraft, or automotive applications or as power supplies for process technology [64]. The three-switch buck rectifier topology was first proposed in [54]. In [41] and [84], aspects of the system modulation and control have been treated. The application of the topology used as an active filter is discussed in [74]. The addition of a DC-DC output boost-stage has been proposed in [9] in order to maintain 400-V output voltage for a wide input voltage range and for the case of unbalanced mains as, e.g., the loss of one phase.

2.4.1 Basic operation principles

For the derivation of the relative on-times of the three buck transistors S_i (with) the following assumptions are made for clarity and facilitation of calculations:

- The AC-side filter capacitor voltages (u_{c_p} , where $p \in \{1, 2, 3\}$) at the input of the CSR are sinusoidal and in phase with the main harmonic component of voltage.

$$\begin{aligned} u_{c_1} &= \hat{u}_c \cos(\omega t) \\ u_{c_2} &= \hat{u}_c \cos(\omega t - 2\pi/3) \\ u_{c_3} &= \hat{u}_c \cos(\omega t + 2\pi/3), \end{aligned} \tag{2.11}$$

where ω is the network voltage's angular velocity.

- The mains currents are assumed to be equal to the fundamental component of the rectifier input currents.
- The current in the DC output inductor L_{dc} is not affected by the high frequency ripple due to the switching operation.

For achieving ohmic mains behavior also in case of unbalanced fundamental harmonics conditions the explained modulation method can still be utilized, however, additionally the control structure presented in [10] has to be employed. The waveforms of the phase and line-to-line mains voltages are divided into twelve 30wide sectors shown in Fig.2.5. The following calculations are based on the analysis of the first sector which is characterized by the voltage harmonic phase relation. For the remaining sectors the calculations can be accomplished in an similar manner ??.

Accordingly, on AC side, if conditions are favorable, inductor current can appear in an instant of time either in two out of three phases or in none. In this modulation technique, the switches in each converter leg can conduct only one at the time (aside from zero states, where both upper and lower switches are conducting). When the upper leg is conducting it is indicated by '1', when the lower '-1' and when neither '0'. As such the choice whether upper or lower switch of the leg conducts current depends of the reference current

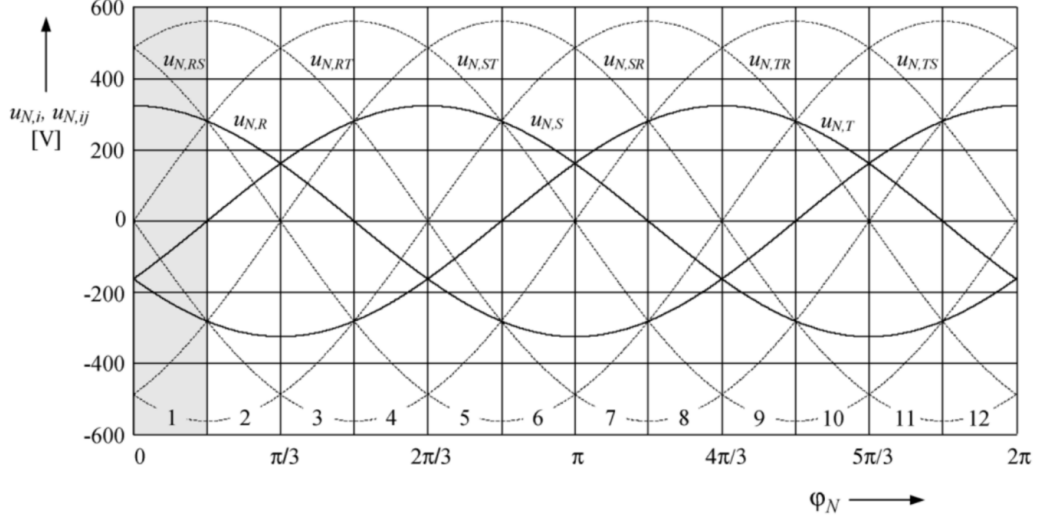


Figure 2.5: Phase voltages u_i , where line-to-line voltages $u_{i,j} = u_i - u_j$, $(i,j) \in \{1,2,3\}$ and sectors 1~12 being defined by the different relations of the instantaneous values of the mains phase voltages for $u = 400V$

vector's sector location. According to the actual switch combination the DC link current shaped by the choke inductance, and distributed to two of the input phases or the freewheeling diode. With this, the input current space vectors can be calculated for each of the before-mentioned switching states. Generally the space vector of three-phase quantities (e.g., for the rectifier input current) are described as:

$$\vec{i} = \frac{2}{3} \left(\vec{i}_a + \vec{i}_b e^{j\frac{\pi}{3}} + \vec{i}_c e^{j\frac{4\pi}{3}} \right). \quad (2.12)$$

Based on 2.14 the corresponding active space vectors in the first sector can be obtained as:

$$\begin{aligned} \vec{i}_{(1,0,-1)} = \vec{i}_1 &= 2i_{dc} e^{j\pi/6} / \sqrt{3} \\ \vec{i}_{(0,1,-1)} = \vec{i}_2 &= 2i_{dc} e^{j\pi/2} / \sqrt{3} \\ \vec{i}_{(-1,1,0)} = \vec{i}_3 &= 2i_{dc} e^{j5\pi/6} / \sqrt{3} \end{aligned} \quad (2.13)$$

The resulting discrete space vectors can be used to synthesize desired current space vector \vec{i}_{ref} .

The modulation methods were evaluated in and choosen for this paper based on [57], which ensures minimum switching-losses, minimum ripple values of the input capacitor voltages and of the output inductor current. According to this modulation, each pulse interval comprises two active states and a free-wheeling state, arranged symmetrically about the middle of the pulse interval (see Table 4.3). For more in depth functional description see Chapter X.

2.5 Asynchronous parallel pattern search

Parallel variants of pattern search to solve nonlinear unconstrained problems of the form of:

$$\min_{x \in \mathbb{R}^n} f(x), \quad (2.14)$$

where $f : \mathbb{R}^n \rightarrow \mathbb{R}$. We assume that the evaluation of f is computationally expensive, hence our interest in using either distributed or parallel computing environments to solve the problem. It needs to be concentrated on the parallelization of the search strategy, rather than on the evaluation of f , though the techniques we discuss here can be adapted to handle problems for which the computation of f also can be distributed. Additionally it is assumed that f is continuously differentiable, we further assume that ∇f is unavailable and not reliable. For such problems, pattern search methods are one possible solution technique since they neither require nor explicitly estimate derivatives.

2.5.1 Parallel pattern search

Lets adopt an infinite sequence of iterations $k = 0, 1, 2, \dots$, with the last iteration noted as $k - 1$ and initialization at 0. It is assumed that the process knows the best point so far as x^{k-1} , where $f(x^{k-1})$ has the global minima of f . Associated with x^{k-1} there is a step-length control parameter namely Δ^{k-1} . Each $i \in \mathcal{P}$, where $\mathcal{P} = \{1, \dots, p\}$ process ends iteration at $k - 1$ by constructing it's trial point and initiating an evaluation of $f(x_i^{k-1} + \Delta_i^{k-1}d_i)$, where $\mathcal{D} = \{d_1, \dots, d_p\}$ is the finite set of directions applied by each individual process. The simultaneous start of the function evaluations at the trial points on each of the p processes signals the start of iteration k . When all of the participating processes are finished with their evaluation of f , they communicate these values to each other and determine the new values of x^k , and Δ^k . If there exists an $i \in \mathcal{P}$, such that $f(x_i^{k-1} + \Delta_i^{k-1}d_i) < f(x^{k-1})$, then $k \in \mathcal{S}$, where \mathcal{S} denotes the successful iterations.

2.5.2 Adding asynchrony

With said above, the general strategy for asynchronous parallel pattern search, from the perspective of a single process $i \in \mathcal{P}$ can be outlined:

1. Evaluate $f(x_i^{best} + \Delta_i^{best}d_i)$.
2. If $f(x_i^{best} + \Delta_i^{best}d_i) < f(x_i^{best})$, then broadcast result to all other processes.
3. Update local values x_i^{best} and Δ_i^{best} based on the current local information.
4. Repeat.

The price payed is that each process has its own notion of the best known point seen so far, as well as its own value for Δ^i . Any success on one process

is communicated to all other processes participating in the search, but the successful process carries on from its new best point without waiting for a response from the other processes. By adding a few mild conditions, the global convergence of the search can be still ensured [1]. Instead of indexing based on a notion of iterations, we switch to indexing based on time step, letting the set $\mathcal{Q} = \{1, 2, \dots, q\}$ denote the index of steps. Thus x_i^q is used for the best point known to process i at time step q , and similarly, Δ_i^q . So if process i starts a function evaluation at time step q , the trial point at which the function evaluation will be made at $x_i^q + \Delta_i^q d_i$. Further worth mention, that time steps are assumed to be of fine enough resolution so that at most one function evaluation finishes per process per time step.

Lets define two sets that satisfy $\mathcal{Q} = \mathcal{S}_i \cup \mathcal{U}_i$, and $\mathcal{S}_i = \mathcal{I}_i \cup \mathcal{E}_i$, where \mathcal{S}_i is the set of all time successful steps on process i , \mathcal{I}_i is the set of internal successes, \mathcal{E}_i is the set of external successes, and \mathcal{U}_i consists the unsuccessful steps respectfully. An internal success, where the process finds itself the minima, the external success is where the process is updated externally by the minima. Further $\mathcal{C}_i \in \mathcal{U}_i$ is defined as the set of time steps where Δ_i^t is reduced. All the above cases ($\mathcal{U}_i \setminus \mathcal{C}_i$) no action is performed.

The updating functions allow us to give the following general definitions for x_i^q and Δ_i^q . For every $q \in \mathcal{Q}$, $q > 0$, the best point for the i^{th} process defined to be:

$$x_i^q = \begin{cases} x_{\omega_i(q)}^{\tau_i(q)} + \Delta_{\omega_i(q)}^{\tau_i(q)} d_{\omega_i(q)}, & \text{if } q \in \mathcal{S}_i \\ x_i^{q-1}, & \text{otherwise} \end{cases}, \quad (2.15)$$

with the initialisation $x_i^0 = x^0$, where $\omega_i(q)$ is the generating process index for the update time at step q on process i , and $\tau_i(q)$ is the time index for initialization of the function evaluation, that produced the update at time q on process i . For every q the step length control parameter Δ_i^q defined to be:

$$\Delta_i^q = \begin{cases} \lambda_{\omega_i(q)}^{\nu_i(q)} \Delta_{\omega_i(q)}^{\tau_i(q)}, & \text{if } q \in \mathcal{S}_i \\ \theta_i^q \Delta_{\omega_i(q)}^{\tau_i(q)}, & \text{if } q \in \mathcal{C}_i \\ \Delta_i^{q-1}, & \text{otherwise} \end{cases}, \quad (2.16)$$

with the initialization $\Delta_i^0 = \Delta^0$, where $\nu_i(q)$ is time index for the completion of the function evaluation that produced the update at time step q on process i , and θ_i^q and λ_i^q are choosen. With the following pattern followed, the minima of f shall eventually reached, in an undetermined steps [47].

2.6 Quadratic optimization and model predictive control (MPC)

Philosophically MPC reflects human behavior whereby we select control actions which we think will lead to the best predicted outcome (or output) over some limited horizon. To make this selection we use an internal model of the

process in question. We constantly update our decisions as new observations become available. Hence a predictive control law has the following components:

- The control law depends on predicted behavior.
- The output predictions are computed using a process model.
- The current input is determined by optimizing some measure of predicted performance.
- The receding horizon: the control input is updated at every sampling instant.

2.6.1 Overview on predictive control

Most control laws, say PID (proportional, integral and derivative), do not explicitly consider the future implication of current control actions. To some extent this is only accounted for by the expected closed-loop dynamics. MPC on the other hand implicitly (or explicitly) computes the predicted behavior over some horizon. One can therefore restrict the choice of the current proposed input trajectories to those that do not lead to difficulties in the future.

In order to predict the future behavior of a process, we must have a model of how the process behaves. In particular, this model must show the dependence of the output on the current measured variable and the current/future inputs. This model does not have to be linear (e.g. transfer function, state-space) and in fact can be just about anything. A precise model is not always required to get tight control, because the decisions are updated regularly. This will deal with some model uncertainty in a fairly fast time scale. The decision on the best control is thus continually updated using information from this comparison [72].

This way, predictive control methods based on a model are optimal regulators, with a defined cost function on a defined and encompassed prediction horizon with restrictions [N9], [N25], [N4], [N16], [N55]. The control signal is calculated over a defined horizon, but from the sequence of applicable control signals only the first one is used in the next sample. This procedure is repeated according to the principle of the moving horizon, using new iterations, as such provides the reaction in each sample. This method was developed for systems with physical restrictions, in the first stage for the control of chemical processes in the oil industry, then it was applied to various rapid processes from automotive or power electronics industry [N1], [N13]. By default the optimization problem can be solved, for each sample, or explicitly using the multi-parameter programming techniques (mp-LP, mp-QP) presented in [N-ANNEX 1], over a well-defined parameter space. MPC example

2.6.2 Constrained optimal control

In practice most MPC algorithms use linear models because the dependence of the predictions on future control choices is then linear and this facilitates

optimization as well as off-line analysis of expected closed-loop behavior. However, nonlinear models can be used where the implied computational burden is not a problem and linear approximations are not accurate enough. It is also important to note here the comment fit for purpose. In predictive control, the model is used solely to compute system output predictions, so the model is fit for purpose if it gives accurate enough predictions. The effort and detail put into modelling stage should reflect this. Let us assume that the system is linear and time-invariant (LTI):

$$\begin{aligned} x(t+1) &= Ax(t) + Bu(t) \\ y(t) &= Cx(t) \end{aligned} \quad (2.17)$$

with the restrictions:

$$Ex(t) + Lu(t) \leq M \quad (2.18)$$

where $t \geq 0$ defines the time instance and $\mathbf{x} \in \mathbb{R}^n$, $\mathbf{u} \in \mathbb{R}^m$, $\mathbf{y} \in \mathbb{R}^p$ are the states, inputs and outputs of the system respectively.

We define the following cost function to optimize:

$$J(U_n, x(0)) = \|Px_N\|_p + \sum_{k=0}^{N-1} \|Qx_k\|_p + \|Ru_k\|_p \quad (2.19)$$

The optimization problem 2.19 applies with restrictions as follows:

$$\begin{aligned} J^*(x(0)) &= \min_{U_N} J(U_n, x(0)) \\ a.i. \quad &Ex_k + Luk \leq M, k = 0, \dots, N-1 \\ &x \in X_f \\ &x_{k+1} = Ax_k + Bu_k, k \geq 0 \\ &x_0 = x(0) \end{aligned} \quad (2.20)$$

where N is the defined horizon, $x \in X_f$ is the set of terminal states, $U_N = [u_0, u_1, \dots, u_{N-1}] \in \mathbb{R}^s$, $s = m \cdot N$. In case of $p = 2$ (Euclidean norm) $Q = Q' \geq 0$, $R = R' \geq 0$, $P \geq 0$ and in case of $p = 1$, Q, R , and P shall be on maximum rank. As displayed, the MPC approach requires a numerical definition so that a precise calculation can be made, that is, which predicted input trajectory gives the lowest numerical value to the cost. The main requirement is that the cost depends on the future controls and that low values of cost imply good closed-loop performance good being defined for the process. Of course the choice of the cost affects the complexity of the implied optimization and this is also a consideration. For this reason 2-norm (square norm) measures are popular, as optimization is straightforward.

Based on the latter and on 2.19 and 2.20 a classical linear quadratic regulator (LQR) structure can be formulated with finite or infinite horizon [N3], [N20], [N21]. Let us consider the following:

$$p = 2, \{(x, u) \in \mathbb{R}^n + m : Ex + Lu \leq M\} = \mathbb{R}, X_f = \mathbb{R}^n \quad (2.21)$$

In this case the problem can be reduced to an unconstrained optimization with finite horizon with the control law:

$$u^*(k) = K_k x(k), k = 0, \dots, N-1 \quad (2.22)$$

Where the control coefficient of the k^{th} instance is K_k can be given in the following form:

$$K_k = -(B'P_{k+1}B + R)^{-1}B'P_{k+1}A \quad (2.23)$$

The positive semi-definite matrix P_k is the solution of the Riccati equation:

$$\begin{aligned} P_N &= P \\ P_k &= A'(P_{k+1} - Pk + 1B(B'P_{k+1}B + R)^{-1}B'P_{k+1})A + Q \end{aligned} \quad (2.24)$$

whith the initial condition:

$$J^*(x(0)) = x(0)'P_0x(0) \quad (2.25)$$

If we choose $N \rightarrow \infty$ and assume that (A, B) are controllable and (A, B) are observable, the optimization problem becomes an infinite horizon LQR whose solution can be written as:

$$u^*(k) = K_k x(k), k = 0, \dots, \infty \quad (2.26)$$

As such:

$$K_k = -(B'P_\infty B + R)^{-1}B'P_\infty A \quad (2.27)$$

with P as the unique solution of the Riccati equation:

$$P_\infty = A'(P_\infty - P_\infty B(B'P_\infty B + R)^{-1}B'P_\infty)A + Q \quad (2.28)$$

These are the basis of model predictive control (MPC). For introduction let us consider the principle of moving horizon (Receding Horizon). Optimization over a finite horizon has the following disadvantages:

- Unforeseen problems may occur after the fixed optimization horizon, which may cancel the sequence of order for the calculated finished horizon.
- After reaching the time defined by the horizon, the law of command is no longer optimal.
- Finite horizon optimization is usually used because of the limited computing power is available, and not for theoretical reasons

To prevent this problem, the notion of optimization is introduced on a moving horizon. In each sample k , an optimization problem is solved over a defined horizon $k, \dots, k+N$ to calculate the appropriate command sequence, and only the first command is applied. This results in a moving optimization horizon, which eliminates the issues listed before. The Formulation of the

optimal control problem with moving horizon [N14] in the system 2.17 with input and output constraints follows:

$$y_{min} \leq y(t) \leq y_{max}, u_{min} \leq u(t) \leq u_{max}, \quad (2.29)$$

with the cost function to minimize:

$$\begin{aligned} J(U, x(t)) &= x'_{t+N_y|t} P x_{t+N_y|t} + \sum_{k=0}^{N_y-1} x'_{t+k|t} Q x_{t+k|t} + u'_{t+k} R u_{t+k}, \\ a.i. \quad &y_{min} \leq y_{t+k|t} \leq y_{max}, k = 1, \dots, N_c - 1, \\ &u_{min} \leq u_{t+k} \leq u_{max}, k = 0, 1, \dots, N_c - 1, \\ &x_{t|t} = x(t), \\ &x_{t+k+1|t} = A x_{t+k|t} + B u_{t+k}, \\ &y_{t+k|t} = C x_{t+k|t}, k \geq 0, \\ &u_{t+k} = -K x_{t+k|t}, N_u \leq k \leq N_y, \end{aligned} \quad (2.30)$$

where $Q = Q' \geq 0$, $R = R' \geq 0$, $P \geq 0$, (C, A) is observable, [missing text] and $N_u \leq N_y$, $N_c \leq N_y - 1$. One trivial possibility to choose $K = 0$ and P to satisfy the Lyapunov equation:

$$P = A' P A + Q \quad (2.31)$$

This means that after N_u samples the control stops and the system is evolving to an open loop form. It is obvious that the choice only makes sense if the open loop system is stable. The second option would as described in 2.27, and 2.28, but this involves to use an unconstrained control for N_u LQR samples. As a result, the MPC law calculates the optimal command sequence:

$$U^*(t) = \{u_t^*, \dots, u_{t+N_u-1}^*\}, \quad (2.32)$$

and only the first control input is applied:

$$u(t) = u_t^*. \quad (2.33)$$

The optimal control inputs estimated for future samples are not taken into account and the algorithm is repeated on the basis of new measurements or a new estimation of the states.

2.6.3 Stability of MPC

The problem of closed system stability with the predictive control has been extensively studied e.g. in [N97], [N54]. In the first generation of model based controllers, stability was achieved more experimentally by choosing parameters based on previous studies and experiences. In 1988 Keerthi and Gilbert introduced the Lyapunov stability method for discrete systems [N65], and in 1990 Mayne and Michalska for continuous systems [N96].

Let $U \subset \mathbb{R}^n$ be an open set where $0 \in U$. A function $V : U \rightarrow \mathbb{R}$ is called positive (or negative) definite if $V(0) = 0$ and $V(\mathbf{x}) > 0$ (or $V(\mathbf{x}) < 0$), when $\mathbf{x} \neq 0$, and $\mathbf{x} \in U$. Also said function called positive (or negative) semidefinite

if $V(0) = 0$ and $V(\mathbf{x}) \geq 0$ (or $V(\mathbf{x}) \leq 0$), when $\mathbf{x} \neq 0$, and $\mathbf{x} \in U$. Clearly V is a negative (semi-)definite function if $-V$ is a positive (semi-)definite function. So, in many applications the domain of V is $U = \mathbb{R}^n$.

Also it can be said (according to the Sylvester theorem [37]) that the quadratic function:

$$V(\mathbf{x}) = \mathbf{x}^T \mathbf{A} \mathbf{x}, \quad (2.34)$$

is positive definite iff all the leading principal minors of the matrix \mathbf{A} are positive. As such consider the nonlinear system 2.35:

$$\dot{\mathbf{x}} = \mathbf{f}(\mathbf{x}), \quad (2.35)$$

where we assume that $\mathbf{f}(0) = 0$ is a (trivial) equilibrium point of the system. The component functions of \mathbf{f} are denoted by $\mathbf{f}(\mathbf{x}) = (f_1(\mathbf{x}), \dots, f_n(\mathbf{x}))^T$. Let $V : \mathbb{R}^n \rightarrow \mathbb{R}$ be continuously partially differentiable, with respect to all variables. By computing the derivative of the composite function $V(\mathbf{x}(t))$, where $\mathbf{x}(t) = (x_1(t), \dots, x_n(t))^T$ is solution of 2.35:

$$\frac{dV}{dt}(\mathbf{x}(t)) = \frac{\partial V}{\partial x_1}(\mathbf{x}(t))f_1(\mathbf{x}(t)) + \dots + \frac{\partial V}{\partial x_n}(\mathbf{x}(t))f_n(\mathbf{x}(t)), \quad (2.36)$$

where the derivative of V with respect to 2.35 follows:

$$\dot{V}(\mathbf{x}) = \frac{\partial V}{\partial x_1}(\mathbf{x})f_1(\mathbf{x}) + \dots + \frac{\partial V}{\partial x_n}(\mathbf{x})f_n(\mathbf{x}). \quad (2.37)$$

If this function is negative definite then for every solution $\mathbf{x}(t)$ the composite function $V(\mathbf{x}(t))$ is monotone decreasing. Moreover, if $V(\mathbf{x}(t)) \rightarrow 0$ as $t \rightarrow \infty$, then $\mathbf{x}(t) \rightarrow 0$ holds. This is the background of the next Lyapunov theorem:

Suppose $\mathbf{f}(0) = 0$, $U \subset \mathbb{R}^n$, is an open set with $0 \in U$. Let $V : U \rightarrow \mathbb{R}$ continuously differentiable with respect to all variables.

- a) If V is positive definite and \dot{V} is negative semidefinite, then the equilibrium 0 of 2.35 is stable.
- b) If V is positive definite and \dot{V} is negative definite, then the equilibrium 0 of 2.35 is asymptotically stable.
- c) If in every neighborhood of 0 there exists \mathbf{x} such that $V(\mathbf{x}) > 0$ and \dot{V} is positive definite, then the equilibrium 0 of 2.35 is unstable.

This way V is called Lyapunov function if its positive definite and its derivative \dot{V} with respect to 2.35 is negative semidefinite.

In this fashion, by using cost function, as a candidate for Lyapunov function, several methods of analysis have been developed, guaranteeing stability. As basis the unconstrained LQR 2.19 is serving to create the Lyapunov function such as:

$$V(\mathbf{x}) = \mathbf{x}' P \mathbf{x}, P \succ 0. \quad (2.38)$$

In order to test this lets make the following calculation:

$$\begin{aligned} V(x_{k+1}) - V(x_k) &= x'_{k+1}Px_{k+1} - x'_kPx_k = \\ &= k'_kA'PAx_k - x'_kPx_k = \\ &= x'_k(A'PA - P)x_k, \end{aligned} \tag{2.39}$$

where, in order to satisfy the Lyapunov theorem:

$$A'PA - P = -Q, Q \succ 0. \tag{2.40}$$

This is referred to as discrete-time Lyapunov equation, where according to [14] iff P satisfying 2.40, then the system is asymptotically stable. From an optimisation point of view problem 2.20 in compact form:

$$\begin{aligned} \min_U J(U, x) &= F(x_N) + \sum_{k=0}^{N-1} L(x_k, u_k) \\ \text{a.i. } x_{k+1} &= f(x_k, u_k) \\ x &\in X, u \in U \\ x_0 &= x(t) \end{aligned} \tag{2.41}$$

Assuming that the function cost $J(U, x)$ is a Lyapunov candidate, the MPC would be asymptotically make the system stable, if the following conditions are met:

1. There is a terminal set $\Omega \subset X$ so that Ω is also marginalized $0 \in \Omega$ (constraints of states are satisfied in Ω).
2. There is a terminal controller $K(x_k) \in U, \forall x \in \Omega, k = N, \dots, \infty$ (constraints of inputs are satisfied in Ω).
3. The set Ω is invariant for the function $f(x_k, K(x_k))$ which needs to be optimized, so for every $x_0 \in \Omega$, all subsequent $x_{k+1} = f(x_k, K(x_k))$ would remain in Ω .
4. $F(f(x_k, K(x_k))) - F(x) + L(x_k, K(x_k)) \leq 0$, then $F()$ is the Lyapunov function in Ω .

Based on these conditions above, there are several methods of stabilizing the systems with MPC regulators, some of these are presented below [N16].

- **MPC with final state constraint:** Stability is ensured by $x_N = 0$. This imposes that $\Omega = \{0\}$, as such $K(x_k) = 0$ maintains the state of origin. The advantage of the method is that we have a simple constraint, but imposing an equality constraint can lead to difficulties in obtaining the solution.
- **MPC with terminal cost:** This method imposes a zero terminal cost, without imposing restrictions for the final states. This method guarantees stability for large prediction horizons of unrestricted systems.

- **MPC with permissible set restrictions of final states:** For this, it is required to $x_N \in \Omega$. This equality constraint ensures that the controller $K(x_k)$ remains in Ω . This method is also called dual predictive controller, because two regulators are used, one with a moving horizon and one with stabilization of $K(x_k)$.
- **MPC with permissible set restrictions on final states and terminal cost:** Combined method, and widely used because it encompasses the advantages of previous methods.

There are also stabilization methods such as infinite horizon MPCs or sub-optimal MPC regulators, but we do not detail these methods because they are not used in the thesis.

2.7 Explicit model predictive control (EMPC)

The problem 2.30 can be transformed into a multi-parametric quadratic programming (mp-QP) problem. Such an approach involves solving the problem "offline", i.e. explicitly for the defined state-space with considering given constraints. By solving the optimization offline, critical regions are obtained, where each region corresponds to an optimal command that can be expressed as a function tuned by system states. Therefore the real-time regulation of the system is reduced to the identification of the critical regions corresponding to the measured state and the application of the optimal control input stored in a table. This method has revolutionized the use of the MPC method for systems with high dynamics, in particular for reduced order systems. The disadvantage of the method is that the number of critical regions increases exponentially with an increasing system order. The following shows the transformation of MPC into mp-QP. Let us assume an optimization problem described by 2.30. The evolution of the subsequent states is calculated based on a mathematical of the system, according to the relation:

$$x_{t+k|t} = A^k x(t) + \sum_{j=0}^{k-1} A^j B u_{t+k-1-j} \quad (2.42)$$

Based on 2.30, and 2.42 the optimization problem becomes:

$$\begin{aligned} V(x(t)) &= \frac{1}{2} x'(t) Y x(t) + \min \left\{ \frac{1}{2} U' H U + x'(t) F U \right\} \\ \text{with restrictions : } &GU \leq W + Ex(t) \end{aligned} \quad (2.43)$$

where $U = \{u'_t, \dots, u'_{t+N_u-1}\} \in \mathbb{R}'_s$, $s = m \cdot N_u$, H is the optimization vector where $H = H' > 0$, and H, F, Y, G, W, E can be directly obtained from A, B, Q, R, P . Let the transformation variable be:

$$z = U + H^{-1} F' x(t) \quad (2.44)$$

the cost function 2.46 becomes:

$$V(x) = V_z(x) + \frac{1}{2}x'(Y - FH^{-1}F')x, \quad (2.45)$$

where $V_z(x)$ is defined as:

$$\begin{aligned} V_z(x) &= \min \frac{1}{2}z'H z \\ &s.t. \quad Gz \leq W + Sx(t) \\ &\text{with restrictions: } S = E + GH^{-1}F'. \end{aligned} \quad (2.46)$$

From 2.46 the standard mp-QP problem can be defined according to [14], and through this transformation the MPC problem can be explicitly obtained.

2.7.1 Storage of critical regions

The issue of iterative model based controllers is that they require a lot of computational resource. The CPU load and required ROM consumption could increase exponentially the longer the more steps the control horizon is calculated. For this reason explicit model based predictive controllers (EMPC) were developed, where only the storage the critical regions and the signal coefficients for each critical region, so the matrices H , K , M , G are required. The on-line part of control consists of searching the critical region for the current states and calculating the necessary inputs for them. One method of storing entire critical regions in order to calculate them, and that is in the order in which the MP-LP or MP-QP problem is resolved. It has the disadvantage, that the search time can be high, as such starting from the top of the list, a linear search is not effective. The efficient method is to store critical regions already in a binary tree [N64], [N111], [N23], [N113]. The method of generating the binary tree is shown in (Fig.2.6.). The basic idea is to sort the critical regions depending on their adjacent sides. For example, in (Fig.2.6.a.) side j_1 divides the state space into two, at the right of it are the regions $X_{2,3,4,5}$ and to the left are the regions $X_{1,2,6}$. They make up the nodes adjacent to the base node I_1 of the binary tree. Next the another side from the space is chosen defined by each node I_2 respectively I_3 , and the algorithm is continued until all the regions in the current node correspond to the same control signal, denoted by F on the shaft in fig. (Fig.2.6.b.) Thus with this search pattern logarithmic search time can be achieved.

The implementation of MPC in explicit form is very efficient up to a certain number of critical regions, because they do not require calculations but only search in a table. For more complex problems or fast systems the method requires longer search time.

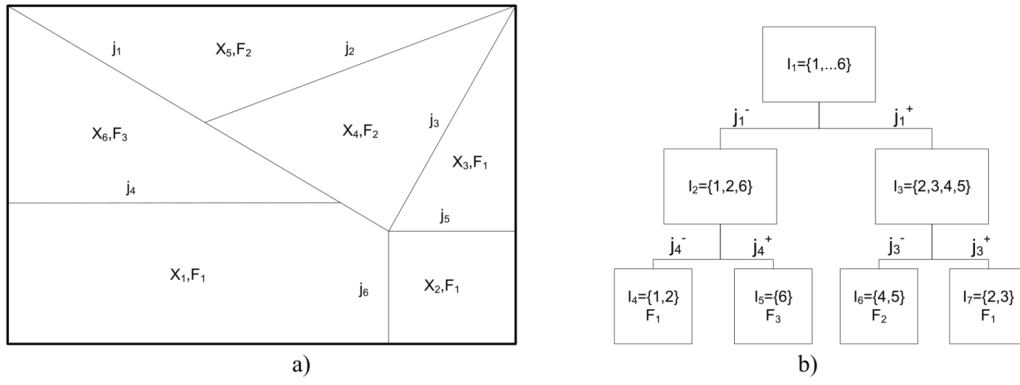


Figure 2.6: Basic search tree of an EMPC where, a) are the critical regions for a space of 2D parameters, b) the related binary tree.

Chapter 3

Voltage unbalance compensation with optimization based control algorithm and asymmetrical inverter structure

In this section a new approach shall be discussed around the phenomena of voltage unbalance in a small domestic network. First the networks structure shall be described, the power electrical system is connected to, as a household supplying, renewable utilising device. Then a control cost-function candidate, the proposed geometrical approach shall be presented, as an indicator of voltage unbalance. Finally, the aforementioned device's topology and control shall be presented based on the geometrical voltage unbalance norm, with the performance results on an unbalanced network.

3.1 Network structure

The examined network is supposed to be the low voltage local transformer area with regular households, depicted in Figure 3.1. The network structure of Figure 3.1 has been implemented in SimulinkTM environment for simulation based experiments. Most of the households represent a single phase load with resistive inductive and capacitive properties while some of them are symmetric three phase ones. There might also be some households with domestic power plant, they are not only loads but also represents distributed generators. Furthermore, it is assumed that the households located on a domestic size grid tie inverter are also provided with battery storage capacities. Commercially available inverters are capable of optimizing the working point and charging current of the system, while the ability of power quality improvement is far not typical - it is in experimental phase in some cases, e.g. [31].

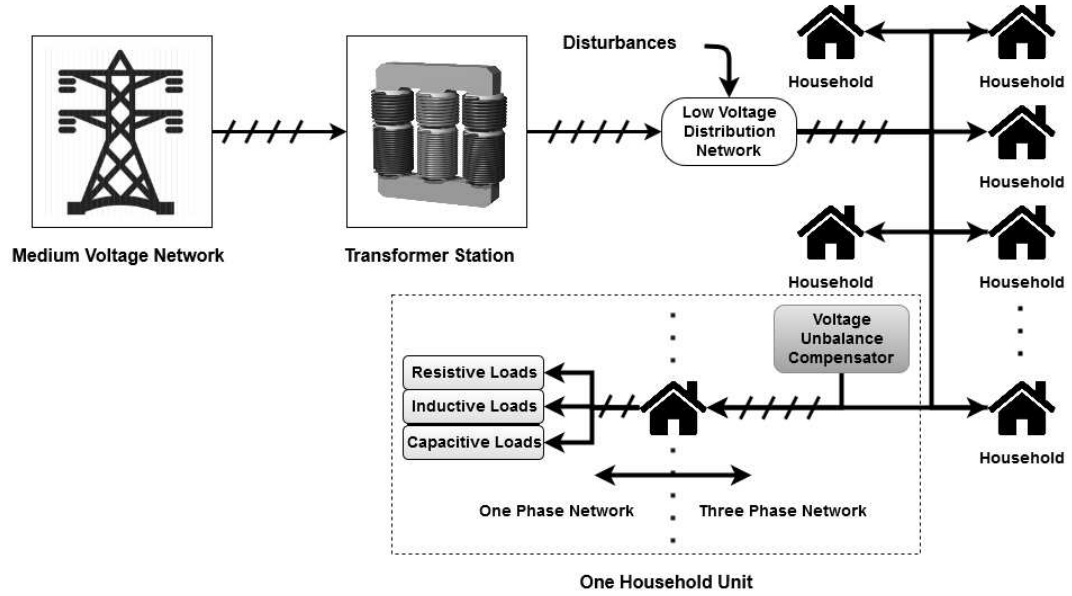


Figure 3.1: The simplified structure of a three phase four wire low voltage network. The transformer station acts as transition from the medium voltage power grid to the low voltage network. The several regular households are representing the main loads of the network. The transformer and the loads are connected with power line sections infected by inductive and resistive disturbances and capacitive couplings. Domestic powerplants can connect to any connection point within the low voltage network, via an appropriate inverter - either to the three phase sections using a three phase inverter or to a single phase using a single phase inverter.

3.2 Proposed geometrical indicator

As discussed in section 2.1.1, the indicators of voltage unbalance result very different measures for the same circumstance. Additionally most of them neglecting the phase differences of voltage vectors compared to the ideal, and even the currently used VUF calculated by 2.8 is not taking zero sequence components from the Foresque method [25]. There were attempts to close the gap with the CVUF norm shown in 2.9, where the complex component is also considered, but this makes this a clumsy candidate for control design, since two components (real and complex part) shall weighted and applied. This begs the question, how could voltage unbalance be measured loss-less, but resulting one (conveniently quadratic-like) value, easily applicable for minimization algorithm

Hence can be stated that every difference between the ideal and the measured voltage in both amplitude phase and sub-harmonics causing a form of voltage deviation. The problem can also be investigated from a geometrical point of view as it is depicted in Figure 3.2. The three-phase voltage system's phasor diagram contains three phase-to-neutral voltage vectors which can be regarded as the points of a triangle (similarly, the three line-to-line vectors can play the role of the edges of the triangle). The two triangles (i.e. the ideal and the

actual ones) always intersect except from very extreme and physically meaningless cases. The area where the two triangles do not cover each other (i.e. the difference of their union and intersection) can be used as a norm of voltage quality. In fact it is computationally more demanding compared to the previous methods, but takes every deviation into consideration [59], [60]. The calculation of error is given by (3.1).

$$G = \text{Area of } (\triangle_{Ideal} \cup \triangle_{Real} - \triangle_{Ideal} \cap \triangle_{Real}), \quad (3.1)$$

\triangle_{Ideal} indicates the triangle spanned by the ideal voltage vectors and \triangle_{Real} the triangle of real voltage vectors. Difference of the ideal and the real triangle's union and intersection defines the norm G . Basically, the algorithm calculates the symmetrical difference of the triangles, stretched from three phase ideal and real voltage vectors.

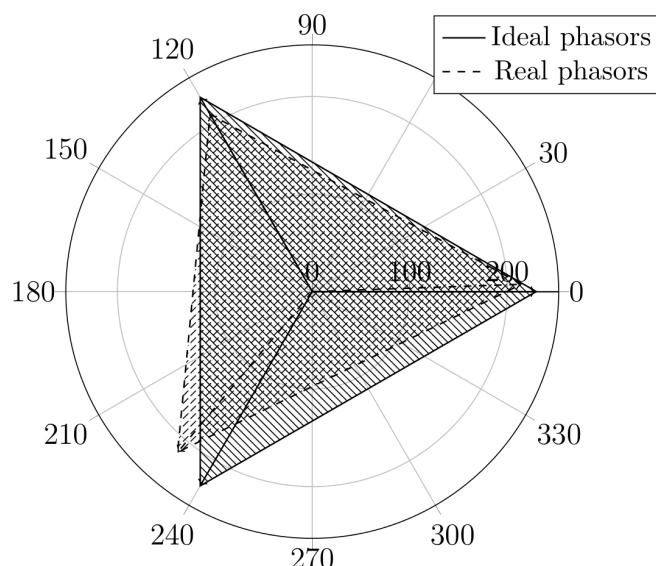


Figure 3.2: The triangles spanned by the ideal and the actual voltage phasors. The extent of voltage deviation on the network can be measured by the sum of areas where the two triangles are not overlapping.

3.3 The method's additional content compared to VUF

When using a new method for calculation and cost function it is reasonable to test it's usability against the prevalent or regulated method the voltage unbalance factor (VUF) defined by the International Electrotechnical Commission, as discussed in section 2.1.5. In this case the geometrical norm's utility (3.1) against the VUF (??) value shall be examined.

The geometrical norm was validated experimentally, by investigating the correlation between the regulated (??) and geometrical (3.1) norms subjected to

random, uniformly distributed unbalance on the voltage vector amplitude and phase values with 20 V amplitude and $1/300 \cdot \pi$ rad phase variance (Fig. 3.3, and Fig. 3.4).

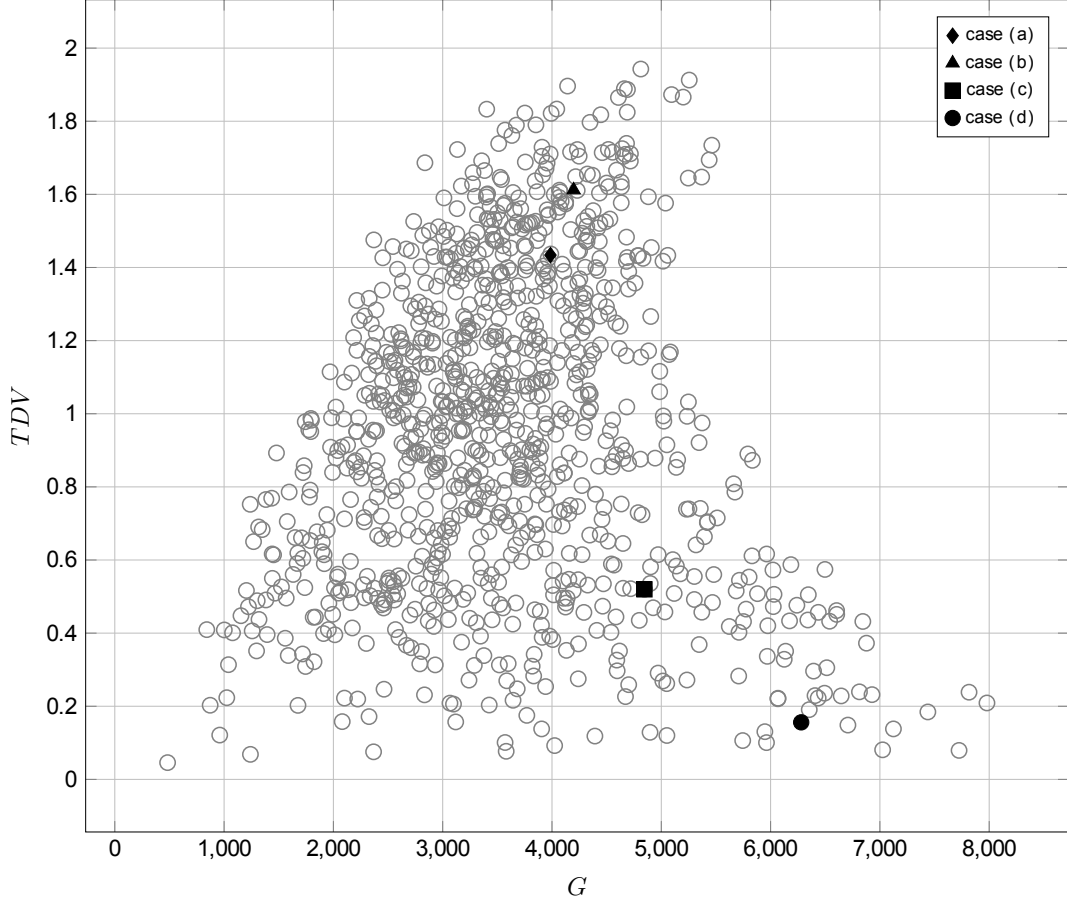


Figure 3.3: Correlation between the geometrical voltage unbalance indicator G and the regulated voltage unbalance indicator TDV using 1000 samples. In every iteration each three phase voltage vector's amplitude and phase values changed randomly, according to uniform distributions with ± 20 V and $\pm \frac{1}{3}\pi \cdot 10^{-2}$ rad variance. It can be seen, that the geometric norm contains more information than the classical one. The four asymmetry cases of Figure 3.5 are denoted by black symbols on the picture. It is apparent, that in case (c), and (d) the G norm holds additional information than the TDV .

Although there is correlation between the two norm values in the general case, but for some situations the regular method indicates low, while geometrical norm still indicates high value.

On Figure 3.5a dominant phase deviation can be observed, while Figure 3.5b shows amplitude deviation but with opposite direction. When there is such deviation on the grid both indicators present almost identical results. On 3.5c there is still observable unbalance (two phase deviate stronger than the third in terms of amplitude), but the correlation is significantly lower. In the last case in the lowest correlation area, amplitude deviation is present, but the deviation direction is identical on all phases (balanced over-voltage or under-

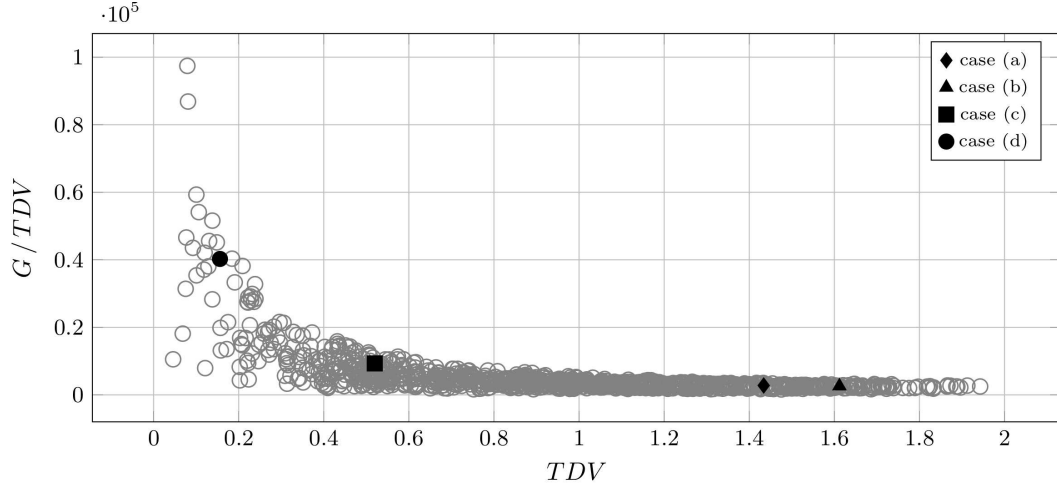


Figure 3.4: Itt a .eps converzio nem lett valami jo, javitani kell! Correlation between the regulated unbalance indicator and the fraction of geometrical and regulated indicator. It can be seen that there is a functional connection between the two values.

voltage)(Figure 3.5d). The regular method indicates very low values. In this case other methods are utilised in parallel in terms of network diagnostics to detect the under-voltage phenomena. [7].

To clarify this, the regular norm's calculation method needs to be investigated. The symmetrical component mutual impedance matrix on a three phase connection point is given by (3.2),

$$\begin{aligned} Z_s &= \frac{1}{3} \begin{bmatrix} 1 & 1 & 1 \\ 1 & \alpha & \alpha^2 \\ 1 & \alpha^2 & \alpha \end{bmatrix} \cdot \begin{bmatrix} Z_{aa} & Z_{ab} & Z_{ac} \\ Z_{ba} & Z_{bb} & Z_{bc} \\ Z_{ca} & Z_{cb} & Z_{cc} \end{bmatrix} \cdot \begin{bmatrix} 1 & 1 & 1 \\ 1 & \alpha^2 & \alpha \\ 1 & \alpha & \alpha^2 \end{bmatrix} = \\ &= \begin{bmatrix} Z_{00} & Z_{01} & Z_{02} \\ Z_{10} & Z_{11} & Z_{12} \\ Z_{20} & Z_{21} & Z_{22} \end{bmatrix}, \end{aligned} \quad (3.2)$$

where Z_s is the symmetrical component mutual impedance matrix, and $\alpha = e^{j\frac{2}{3}\pi}$. If there are both negative and zero sequence symmetrical components present on the network, the dominant part of the voltage drop's negative and zero sequence can be calculated as follows (3.3).

$$\begin{aligned} \Delta U_2 &\approx Z_{21}I_1 + Z_{22}I_2 \\ \Delta U_0 &\approx Z_{01}I_1 + Z_{00}I_0, \end{aligned} \quad (3.3)$$

ΔU_0 , ΔU_1 , ΔU_2 are the voltage drop's zero positive and negative sequence components, I_0 , I_1 , I_2 are the current's drop's zero positive and negative sequence components, and Z_{00} , Z_{01} , Z_{21} , Z_{22} are mutual impedances, respectively. (If there is only positive and negative sequence present, then the right hand side's second term is zero.) As such, the indication of negative and zero sequence present the network calculates (3.4):

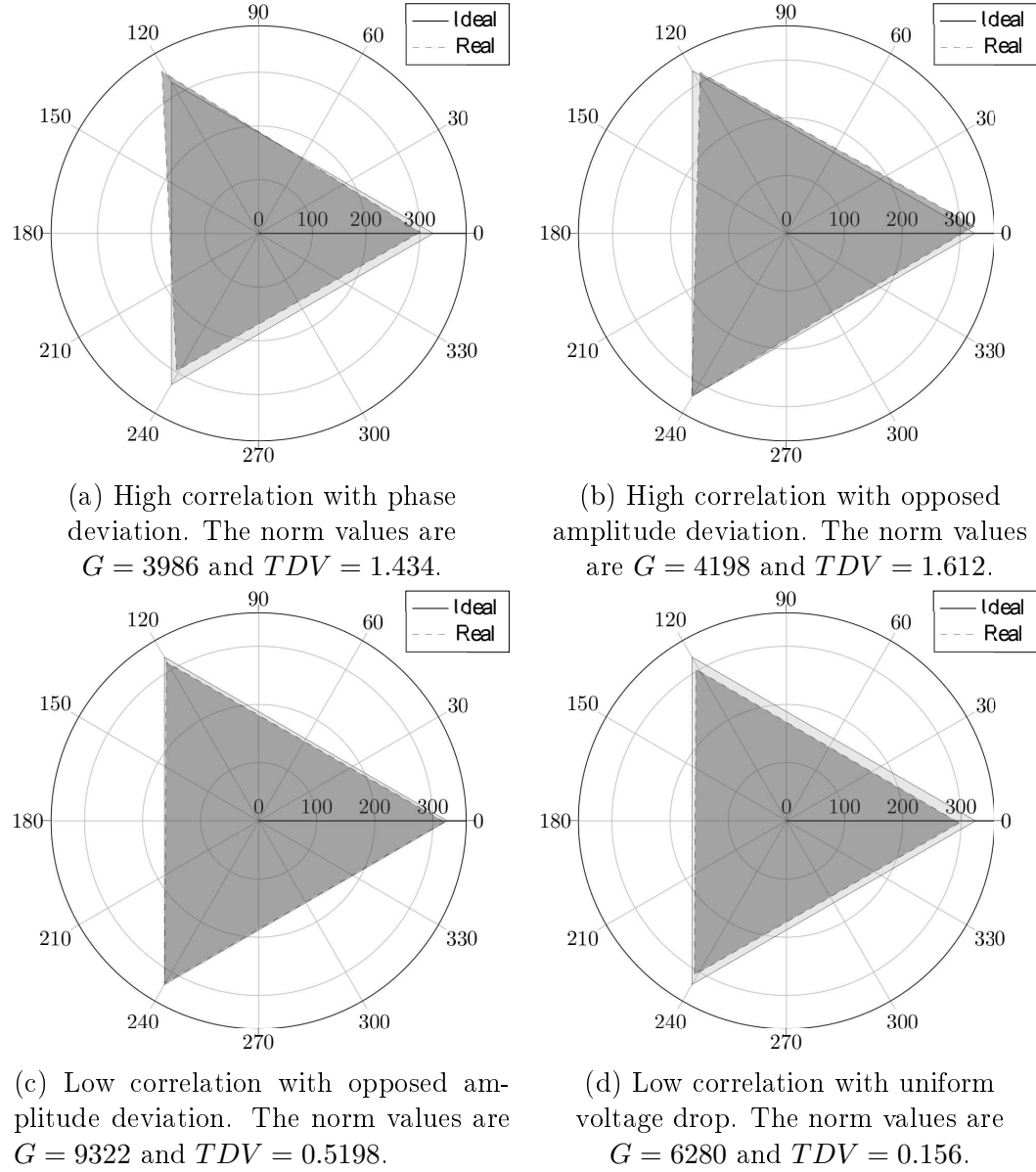


Figure 3.5: Four distinct cases of voltage triangles examining correlation between the regular TDV and geometrical G method.

$$\begin{aligned} m_{21} &= \left| \frac{Z_{21}}{Z_{11}} \right| \times 100 \\ m_{01} &= \left| \frac{Z_{01}}{Z_{11}} \right| \times 100, \end{aligned} \quad (3.4)$$

where m_{21} is the negative sequence factor which is identical to the TDV (??), and m_{01} is the zero sequence factor.

At the previously described balanced over- or under-voltage case the positive sequence value is dominant, so the regular indicator will take considerably lower value. In other words, aside from indicating voltage unbalance, the geometrical method incorporates the balanced deviations as well. In a control design perspective, a general case, where notably highly unbalance values may appear, using TDV as cost function could introduce hidden errors in control due error cancellation. Additionally the geometrical solution checks electrical asymmetry, i.e. the norm of a ± 120 degree rotated version of the ideal three-phase phasor is zero in the geometrical sense. Moreover, the geometrical norm is more sensitive for small scale unbalance, as opposed to the TDV. To summarize, the geometrical indicator a more suitable solution for a more general case indicator, and a good candidate for cost function in optimal control design.

3.4 Unbalance compensation

Based on the proposed measures on voltage unbalance indication, it is possible to formulate some power quality related aims, or demands for the domestic size generator units implemented in a complex power electrical system, capable of supplying a household, with both renewable and network supplied energy, and lowering voltage unbalance as well.

3.4.1 Problem statement

The voltage and current unbalance presents in the three phase low voltage transformer area causes additional power loss inside the medium voltage/low voltage transformer and in the transportation line wires too. It also has undesired effects in certain three phase loads, mainly rotating machines where it causes torque reduction and pulsating torque effect. Large scale unbalance can activate automatic protection functions of electricity dispatch system causes power outage. This is unpleasant for the customers and adds maintenance cost to the service provider. These negative effects lower the electric power quality and rises the cost of electrical energy and rises the carbon footprint of our everyday life. The paper's aim to propose a model and control for a three phase instrumentation, which can compensate these undesirable effects, lower or eliminate the voltage and current unbalance to lower the power losses and the CO₂ emission and increase power quality not only at the connection point but in the whole low voltage transformer area. *It is important to note, that this power quality improvement can be achieved without any significant added cost.* The future aim is to integrate this function into an existing three phase photovoltaic inverter device connected to the low voltage grid, and a complex energetic system is able to inject the renewable energy to the transportation

network, can store the electrical energy from stochastic renewable sources in electrical vehicle batteries or feed the grid from the charged batteries in energy deficit and high demand simultaneous situations. Our new added value is the integrated control algorithm which can highly lower or eliminate the observed unbalance of the network.

3.4.2 Control problem

The above problem statement partially specifies the solution space together with the solution method. The system of interest is the power grid with all the stochastic and nonlinear phenomena present in it mentioned in section 3.1. The input to the system are current signals (one current in the single phase case and three in the three phase setup), which are naturally constrained by the available energy of the household, stored in a battery pack or momentarily generated by the wind or solar generator unit. The response of the system can be either the current or the voltage measured at the connection point of the inverter unit, however, the general legal regulations only allow voltage measurement for consumers. The difficulty of the control problem comes from the fact, that there are no mathematically tractable models of the network can be generated because of its unpredictable and nonlinear features. This means, that in these terms only black-box methods can be applied for this system. For the control aim it is a natural choice to minimize the actual voltage unbalance of the low voltage local transformer area measured (or calculated) at the connection point of the inverter. Several optimization based methods are available for such kind of optimal control problems, e.g. [31] where the only bottleneck is the computational efficiency since the implemented controller has to run on the commercial inverter's hardware (digital signal processor unit).

Asymmetrical inverter structure

For the sake of completeness an asymmetrical inverter was developed in simulation environment, which is capable of carrying out the specified control task. The renewable energy injection is realized increasingly, and applied directly to the three phase low voltage grid with a domestic size photovoltaic power plant as source of power. This can reduce the voltage and current unbalance caused by the stochastic power production of wind and solar sources. More and more manufacturers produce three phase grid synchronized inverters from 5 kW size. These equipments implement accurate symmetrical current feed with a standard three phase full bridge structure, consists of six Isolated Gate Bipolar Transistors (IGBT). The demand is to employ a current source single phase structure with aforementioned controllable switches in section 2.2. This is a standard structure suitable for symmetric harmonic current injection. It has limited capacities to inject not totally symmetric 3 phase current time functions, but Kirchhoff's current law permits only constant zero-sum current time functions injected with this structure. There are examples with this type of asymmetric current injections in the literature [51]. This type of current injections has limited compensation capacity and this is

not enough in most asymmetric production and load cases. In our case we need more general, not specific asymmetric current waveforms, because the proposed control aim assumes the ability of injecting non zero-sum currents. This needs special inverter design structure. We need zero line connection for the differential current. One of the possible solution is to use 3 different full bridge single phase current inverters to supply each phase of low voltage transportation lines [66]. This way it is most sufficient to use bi-directional power flow, with galvanic decoupling, but with a current controlled fashion (shown in section 2.2).

This isolation can be reached with using isolation transformers in the supply side. But we prefer to use it a complex energetic system with specific inside true DC bus system fed from Photovoltaic panel or batteries. We have to isolate at least 2 full bridges with two way DC-DC converters (described in section). This can complicate the physical realization but easy to simulate with two controlled power source. Other possible easy to realize solution to isolate the full bridge outputs connected to three phase lines with isolating transformers. It is recommended due to electric shock protection reasons. Our distant aim to compensate other operational type line failures, such zero current appearing. This isolation method doesn't allow to produce DC current components, thats why we are looking for other design. Possible elegant solution to supplement the standard three phase inverter design with a fourth half bridge for Zero line, building a specific four leg inverter design [63].

Only drawback of this solution is the complex difficult control method of the half bridges, to keep the current sum in zero values in each moment, and to provide the correct current paths inside the inverter. This structure has the lowest production cost, but in the phase of proofing the asymmetry compensation we chose the DC-DC isolated full bridge design for simulation purpose because of the simple control during simulation.

As a further generalization step, the injection of no harmonic current shapes will be necessary in order to decrease the extant Total Harmonic Distortion (THD) of the network. These expectations yield an inverter with new structure suitable for arbitrary current injections without limitations. The design lends similar elements like in [31] by means of battery charge, renewable power point tracking, intermediate voltage, and IGBT bridge control, but in this case the problem requires a three phase solution for the voltage unbalance reduction. The applied structure based on a full bridge IGBT structure used in single phase current injection. Three different IGBT full bridge were connected at the output point, thus our structure has three phase and neutral connection too, to carry out any current form. The disadvantage of this structure is that it needs 12 IGBTs in the output stage as opposed to the 6 IGBTs needed for a classical full bridge structure and needs three galvanically isolated direct current (DC) voltage source for feeding.

The other standard elements, that the inverter design consists:

- Standard maximum power point tracking (MPPT) input stage, to inject the maximum available power from the renewable source to the intermediate voltage capacitor with a simple controlled boost converter

3.4. UNBALANCE VOLTAGE UNBALANCE COMPENSATION

- A half bridge current controller to charge or deploy the battery pack connected to the complex energetic system for energy storage and energy unbalance compensation
- Intermediate voltage controller
- Universal three phase output stage with 3 single phase full bridge IGBT current injector and 2 high current DC-DC converter

This is suitable to inject any necessary current shape to the low voltage three phase grid connection even DC currents too. Later a power loss and production cost analysis will be necessary if the built structure will be suitable for asymmetric compensation of low voltage transformer area.

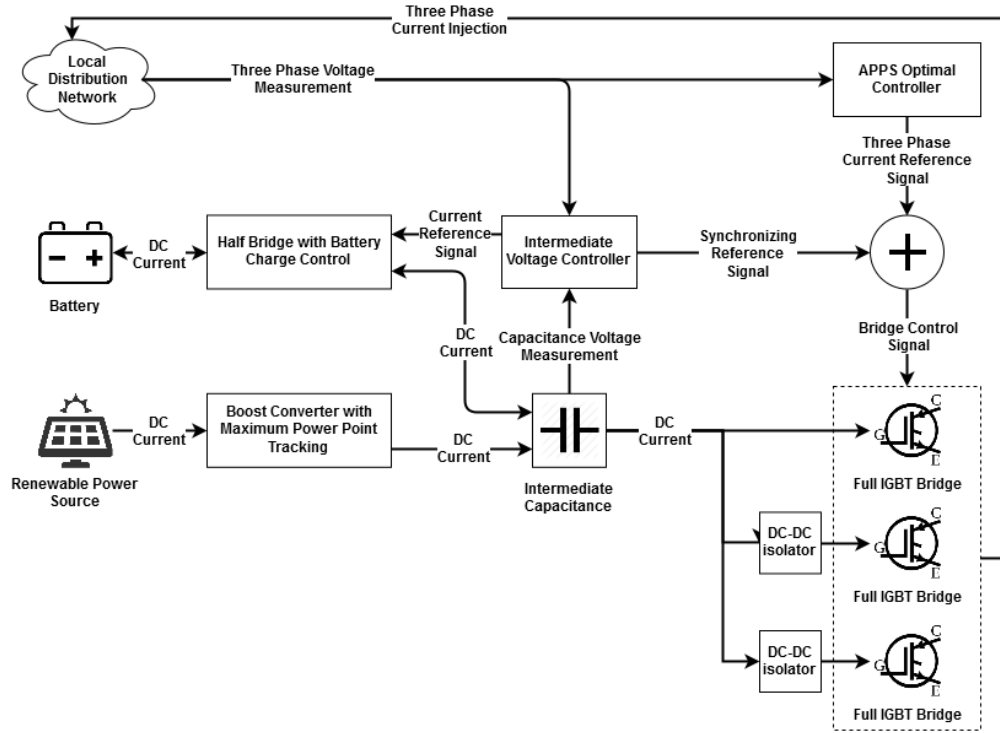


Figure 3.6: The asymmetrical inverter design, which applies three single phase full bridge IGBT current injector to create the injected asymmetrical current shapes for voltage unbalance compensation.

Of course there is a possibility that there is no renewable power available for a longer period of time and the battery completely loses its charge. In this case the system should work merely with the power of the connection point but with zero energy balance. This states to operate two controller with semi-opposite control goals. The optimization based controller requires current injection while the intermediate voltage controller (Figure 3.6) keeps the inverters energy balance. Although for this operation some of the control's performance should be sacrificed, unbalance compensation could be achieved even without external renewable power, and energy storage at a minimum power requirement.

Measurements from a real unbalanced network

The measurements took place at the Faculty's building, where a common 400 V connection point was investigated as the behaviour of the network. The three phase 230 V line-to-ground voltages has been transformed to 6 V to be effectively measurable time domain with high performance NI-USB DAQ on 10ksample/s. Because of the limited computational capacity only a 10 second measurement was made in every hour. The measurements then has been merged and smoothed to eliminate the inter-measurement transients.

Afterwards, the measurement data has been used as the input of a micro-grid segment of the Matlab/Simulink model, to test the controller and inverters structure's performance in quasi-realistic circumstances. The controllers performance on the simulated microgrid's network loss reduction can be observed on Figure 3.11 and Figure 3.12. The measurement output is connected to a modeled three phase load and network system, consisting of symmetrical loads and network segments between them. Further artificial load unbalance is not necessary since the network's unbalance is already present. This structure enables to show that any point the inverter is connected could serve as quality restoration such unbalance compensation at this case. Our future plan is to set up multiple devices on different connection points.

3.4.3 Optimization based control algorithm

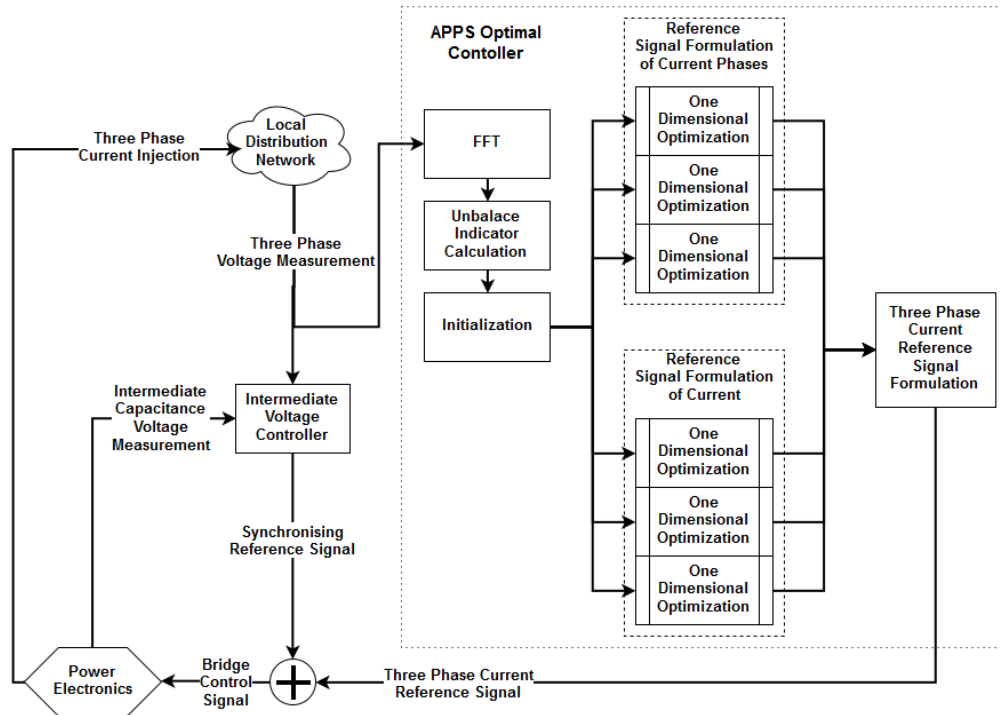


Figure 3.7: The optimization algorithm implemented for current control. A one dimensional linear optimization step is being solved in each dimension of the six dimensional parameter space, iteratively.

The problem is that, the exact mathematical relation is nonlinear because the nonlinear, and highly time variant loads of the network, we should use a control strategy to cope this nonlinear and time variant energy system. For this purpose we chose an asynchronous parallel pattern search method (APPS) which could be able to control our scenario [38]. The methodology and formulation of the APPS method is described in section 2.5. We applied a variant of the gradient method that is a first-order optimization (minimization) algorithm for a multivariate function $f(x)$. The point $x(q)$ corresponding to the local minimum can be calculated from the negative gradient $\nabla f(x)$, that gives the value and direction of the corresponding step in the parameter space. The next step is made in the direction of gradient with the proper sign. This sequence of steps, ideally, converges to local multivariate extreme value $x(q)$ of the function (3.5).

$$x^{(q)} = x^{(q-1)} - t_q \nabla f(x^{(q-1)}), \quad (3.5)$$

where $q \in \mathbb{N}$, and t_q resembles the step time of the algorithm. The controlled electrical system is described by multivariate non-linear differential equations, the optimization of which is infeasible to derive using the differentiation of an error function. Therefore, the optimization methods based on direct differentiation are not applicable. In such cases, when high computational power is needed for performing long time-consuming simulations, the APPS method can be utilized. The search pattern p is based on the sampling of the error function (selected norm) on a "grid", and it corresponds to variables or subsets of variables in each point in the independent variable or parameter space easily. At the same time, the norm values at these points can be calculated independently if $\Delta_q > 0$, using (3.6).

$$\begin{aligned} x^{(q+1)} &= x^{(q)} + \Delta_q d_i \\ \text{if } f(x^{(q)} + \Delta_q d_i) &\leq f(x^{(q)}), \end{aligned} \quad (3.6)$$

The parameter is $x(q) \in \mathbb{R}^n$, and the search pattern $p \in \mathcal{D} = d_1, \dots, d_n$ is taken from a predefined finite set. In this case, the error function values should be calculated for each pattern p in the set \mathcal{D} . If the error function is not decreasing in any of the directions, then the step size should be reduced (e.g. by half). As the competing directions are different, if there is not enough computing power available for direction vector p , synchronization should not be maintained. In this case we are talking about the asynchronous case. In the case of our controller, an individual p vector is defined for each output variable, and the optimization was performed in each direction asynchronously and shifted in time. Most likely, the error function has a single local minimum as a symmetric amplitude and phase values. Approaching the minimal value of norm, the controller uses adaptive increments that are proportional to the norm itself. Because of the complex interactions between the components of the controller, only one parameter is changed at a time, even if the values of the amplitude and phase components in specific time slot changes. The algorithm moves along the six axes of six separate time slots close to the local minimum of the error function.

Unlike other similar approaches, e.g. [78], the explained optimal controller does not rely on a measured current signal (which varies according where the measurement took place on the grid and renders the global optimization unreliable) but rather measuring and analyzing the voltage unbalance via the proposed indicator and optimizes the voltage shape, the latter of which depends on the nonlinear distortion of the whole low-voltage transformer area and determines additional power losses. The controller's performance was compared to a non compensated network, and a network consisting synchronized symmetric power intake from a regular inverter.

In each iteration only one physical value is changing on the six dimensional parameter field, which consists of the three amplitude and three phase values. If the change effects with cost function reduction (the reference norm's normalized value), the controller holds the new value of amplitude or phase for the controlled current sources (Figure 3.7). The advantage of this controller structure that is not necessary to know the controlled value's behavior well, like we could not determine the number and type of the other loads on the network [59]. There are however two disadvantages. First is the low speed of control, due to the several necessary iterations (depending on the circumstances) to find the optimal directions in the parameter space, and the serial nature of interventions and norm calculations. The second comes from the method itself since the controller may stuck in local minima.

3.5 Discussion

write stuff here..

3.5.1 Dynamical simulation based experiments

Simulation's PC parametes, ML/Simuling version

In order to be able to investigate the proposed optimization based unbalance reduction control structure with the three phase inverter on a low voltage local grid, all the elements of this complex electrical system (including the photovoltaic source, the inverter, the battery and the nonlinear local grid with different types of loads) has been modeled in Matlab/Simulink environment. The primary aim of the simulation based experiments were to serve as a proof of concept for the proposed complex control structure.

3.5.2 Performance analysis

The aim of performance analysis is twofold. First of all, the proposed voltage unbalance indicator has to be investigated in the control structure as the cost function of the optimization based controller, and on the other hand, the control structure itself has to be exposed against engineering expectations.

The results of the first experiment can be seen in Figure 3.8 where the geometrical norm 3.1 has been used as the voltage unbalance indicator and the

cost function for the optimizer. The dashed line represents the examined low voltage local network's unbalance norm (G) without the proposed controller implemented in the inverter unit of the domestic powerplant while the solid line represents the compensated network's norm value. The performance of the controller with this norm is apparent, it was able to decrease the network voltage unbalance by approximately 85 %. In this experimental setup the controller has enough input energy due to the batteries and the available solar power.

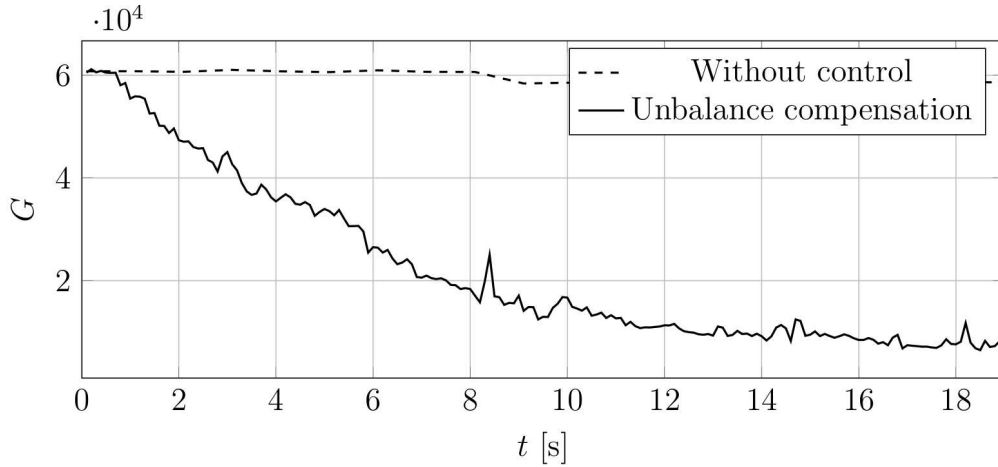


Figure 3.8: Unbalance reduction control system performance with half charged battery and photovoltaic power source available. The underlying unbalance norm is the geometrical one (G) in this experiment. After starting the controller at $t = 0.1s$ the unbalance measure G of the network significantly decrease.

A slightly more challenging situation is investigated in Figure 3.9 where the controller had had to operate without photovoltaic source and batteries. This is called zero balance operation mode when the energy obtained from the network is reinjected in such a way that the unbalance indicators decrease. It can be seen that the performance of the controller is modest than that of Figure 3.8, but it is still acceptable.

Robustness analysis

The robustness of the proposed control structure is an important qualitative property with respect to the time dependent loads present on the network. The robustness of the proposed controller had to be tested via simulation when different types of loads (inductive, capacitive, resistive) had been varied in step changes representing representing the on/off switching the different types of household appliances (motors, switching mode power supplies, electric heaters, etc.). In the experiment depicted in Figure 3.10, a load change has been introduced to the network in every 15 seconds causing the voltage unbalance to jump to a different value (measured in the geometrical norm (3.1)). As it

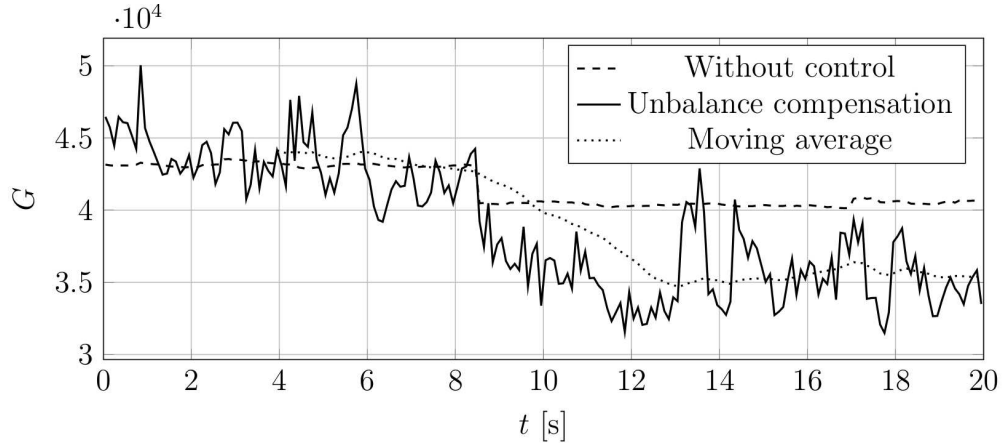


Figure 3.9: Unbalance reduction control system performance without battery and renewable source (zero energy balance operation). The performance reduction is clearly observable compared to the case when external power source is available (Figure 3.8), but as result the voltage unbalance indicator G reduced by the average value of 14.78%.

can be seen in the figure the controller successfully compensates the unbalance after each transient.

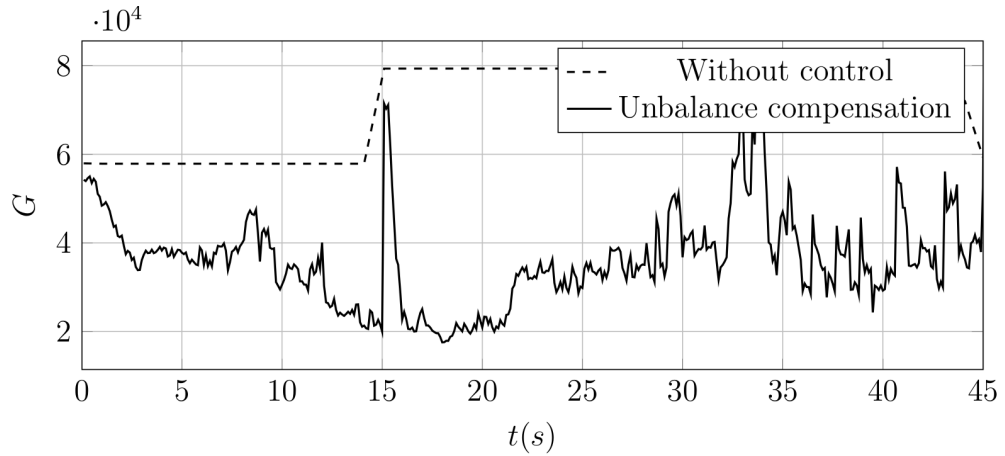


Figure 3.10: Robustness analysis with respect to step type changes in the network load (and voltage unbalance). The unbalance reduction controller successfully compensates the changes in the network voltage unbalance norm (G) value.

3.5.3 Environmental effect

The favorable effects of the proposed unbalance reduction control algorithm, i.e. increase power quality not only at the connection point but in the whole low voltage transformer area, which causes a reduction of the effective power loss and the reduction in the CO_2 emission.

Power loss reduction on the network

Network loss reduction due to the unbalance reduction compensation control is investigated on Figure 3.11 where the simulation experiment was carried out in the circumstance when the renewable source was not shut down (e.g. insufficient amount of sunlight) and additionally the battery was drained completely [59], [60].

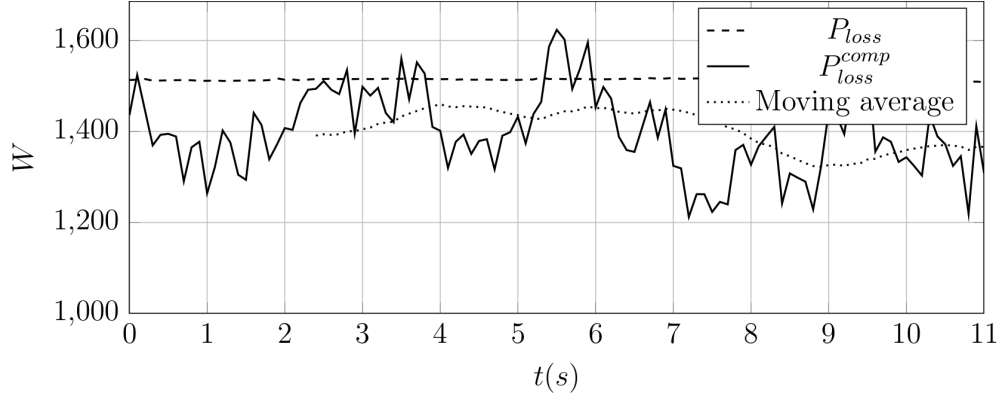


Figure 3.11: Compensation control's loss reduction during zero energy balance operation on the modeled network, where P_{loss} indicates the effective power losses and P_{loss}^{comp} effective power losses during control of the network. As result the network losses reduced by mean 6.5%.

The results show that despite of the negative cross effects of the intermediate voltage controller and the unbalance reduction controller it was possible to find the trade-off between the control goals of the different controllers (maintain zero energy balance for the inverter and decrease the unbalance on the network). The estimated loss reduction in the experimental setup is 6.5%.

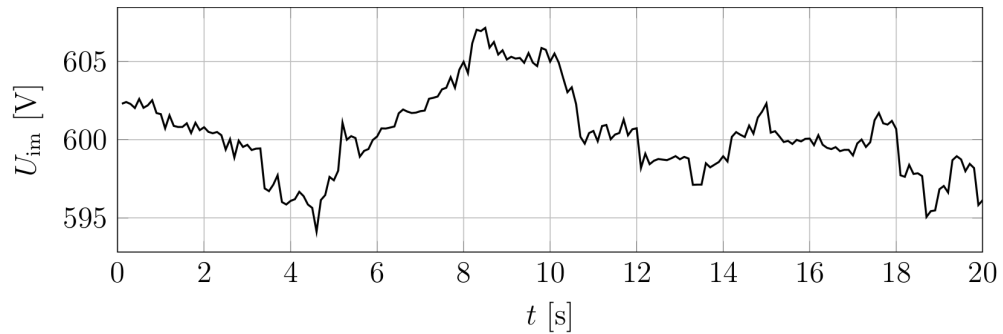


Figure 3.12: Intermediate puffer capacitance's voltage within boundaries (600 ± 10 V), during zero energy balance operation mode of the voltage unbalance compensation controller. U_{im} indicates intermediate the capacitance's voltage.

CO₂ footprint

The fact that this controller enables the reactive power reduction has a favourable consequence, i.e. the power loss or equivalently CO₂ emission and the carbon footprint can also be decreased. The estimated environmental effects of voltage asymmetry compensation can be calculated. Let us assume 3000 kWh for the yearly electric energy consumption an average household and 9.173% for the loss of the distribution network [4]. With the controller the losses on the simulated network are reduced by 6.5%. The calculation follows (3.7)

$$\begin{aligned} P_{loss} &= 3000 \text{ kWh} \cdot 9.173\% \\ P_{loss}^{comp} &= 3000 \text{ kWh} \cdot (9.173 \cdot 0.93)\% \\ \Delta P_{loss} &= P_{loss} - P_{loss}^{comp} \end{aligned} \quad (3.7)$$

where P_{loss} is the assumed network loss per household and P_{loss}^{comp} is the assumed network loss with unbalance compensation control and ΔP_{loss} is the saved energy. According to (3.7), unbalance compensation results in an energy savings of 19.26 kWh. Taking into account the proportion of power currently generated by fossil fuels (coal 17.3 %, gas 38.3% [4], [31]) and the rate of CO₂ emission during electric energy production (1,000 g/kWh from coal and 430 g/kWh from gas), it can be concluded that voltage unbalance compensation could reduce CO₂ emissions by 6504.9 g a year, in an average household.

3.6 Conclusion

The currently used measures of voltage unbalance has been extended in this work with a norm candidate. It is more demanding from the computational point of view but has an interesting feature namely it checks electrical asymmetry, i.e. the norm of a ± 120 degree rotated version of the ideal three-phase phasor is zero in the geometrical sense.

The defined norm is applied as a cost function in the asymmetry reducing controller structure also presented in the paper. Simulations show that the geometrical based indicator can serve as a basis of further research. The suggested controller structure enables the residential users owning a grid synchronized domestic power plant to reduce voltage unbalance measurable at the connection point. The fundamental element of the system is a modified three phase inverter that is capable of the asymmetric injection of any current waveforms to the network. The optimization based control algorithm injects the available energy (as current waveform) in such a way, that the voltage unbalance decreases. This optimization problem is usually constrained by the available renewable energy supplied by the power plant.

The control structure has been tested on a low voltage network model in a dynamical simulation environment consisting of the models of the electrical grid, a domestic power plant, asymmetrical inverter circuit, and different types of loads. Different simulation experiments has been run for each norm and for both the power constrained and unconstrained case. The preliminary results

show that this structure can serve as a residential level voltage quality improvement method for the three phase low voltage network also indirectly reduces the CO₂ emission due facilitating more effective energy usage.

Chapter 4

Constrained, explicit predictive control for current source buck-type rectifiers

As mentioned in section 2.4 current source rectifiers (CSR) play a major role in industrial instrumentation. They are invaluable, where direct power control, torque control, or power injection is required. In this chapter, the modeling and control of such CSR (or buck-type rectifiers), in a model based predictive manner, with explicit partitioning of the state space. The reason of the regular MPC's insufficiency is that power electronic systems require very low time constant to operate smoothly. As such pre-mapping the state-space with applicable control rules gives a great leverage, thus making the possible computational unit much cheaper.

4.1 Modeling

Understandably, model based controllers require the system's model they ought to control, or supervise. In this case the most common structure of a CSR is chosen, with inductive and capacitive filtering on both ends. The differential equations are constructed via Kirchhoff's law and then presented as a state space model for further examination.

4.1.1 Mathematical Modeling of the CSR

The structure of the classical three phase buck-type current source rectifier (CSR) is presented in 4.1. In continuous current mode, the differential equations corresponding to the CSR's inductor currents and capacitor voltages are the following:

$$\begin{aligned} L_{ac}\dot{i}_{ac_p} &= u_p - u_{c_p} - Ri_{ac_p} \\ C_{ac}\dot{u}_{c_p} &= i_{ac_p} - \delta_p i_{dc} \\ L_{dc}\dot{i}_{dc} &= (\sum_{p=1}^3 \delta_p u_{c_p}) - u_0 \\ C_{dc}\dot{u}_0 &= i_{dc} - \frac{u_0}{R_{load}} \end{aligned} \tag{4.1}$$

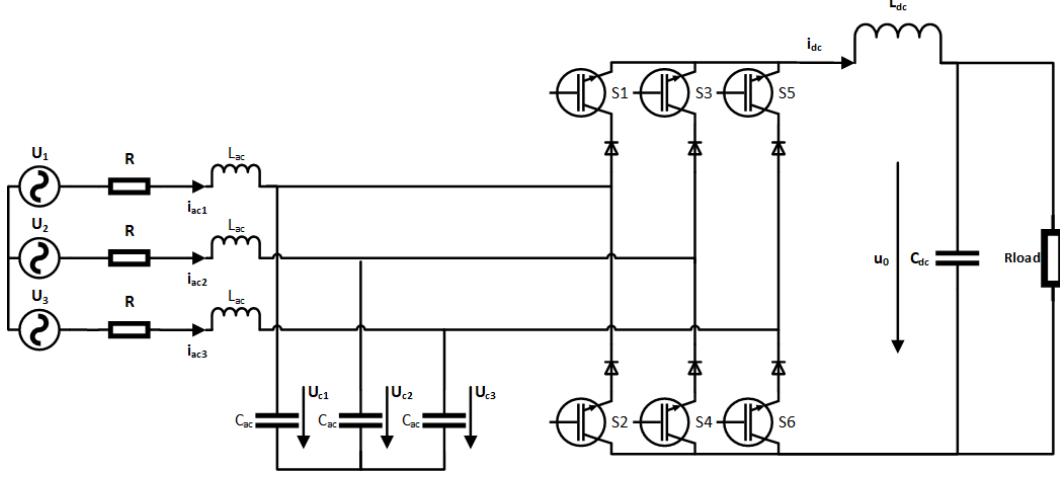


Figure 4.1: Circuit diagram of the three-phase buck-type rectifier with insulated gate bipolar transistors (IGBTs).

where $p \in \{1, 2, 3\}$ is the index of three phases and δ_p describes the conduction state of the rectifier leg p 4.2.

$$\delta_p = \begin{cases} 1 & \text{if the upper transistor is ON} \\ -1 & \text{if the lower transistor is ON} \\ 0 & \text{if both are ON or OFF} \end{cases} \quad (4.2)$$

Using the components in the stationary frame of the space phasors of the three-phase quantities, from 4.1 it results:

$$\begin{aligned} L_{ac} \dot{i}_{ac_\alpha} &= u_\alpha - u_{c_\alpha} - R i_{ac_\alpha} \\ L_{ac} \dot{i}_{ac_\beta} &= u_\beta - u_{c_\beta} - R i_{ac_\beta} \\ C_{ac} \dot{u}_{c_\alpha} &= i_{ac_\alpha} - \delta_\alpha i_{dc} \\ C_{ac} \dot{u}_{c_\beta} &= i_{ac_\beta} - \delta_\beta i_{dc} \\ L_{dc} \dot{i}_{dc} &= 1.5(\delta_\alpha u_{c_\alpha} + \delta_\beta u_{c_\beta}) - u_0 \\ C_{dc} \dot{u}_0 &= i_{dc} - \frac{u_0}{R_{load}} \end{aligned} \quad (4.3)$$

Equation 4.3 is transformed to the synchronous reference frame rotating with the u_{cd} capacitor voltage space vector. The resulting mathematical model is thus:

$$\begin{aligned} L_{ac} \dot{i}_{ac_d} &= u_d - u_{c_d} - R i_{ac_d} + \omega L_{ac} i_{ac_q} \\ L_{ac} \dot{i}_{ac_q} &= u_q - u_{c_q} - R i_{ac_q} - \omega L_{ac} i_{ac_d} \\ C_{ac} \dot{u}_{c_d} &= i_{ac_d} - \delta_d i_{dc} + \omega C_{ac} u_{c_q} \\ C_{ac} \dot{u}_{c_q} &= i_{ac_q} - \delta_q i_{dc} - \omega C_{ac} u_{c_d} \\ L_{dc} \dot{i}_{dc} &= 1.5(\delta_d u_{c_d} + \delta_q u_{c_q}) - u_0 \\ C_{dc} \dot{u}_0 &= i_{dc} - \frac{u_0}{R_{load}} \end{aligned} \quad (4.4)$$

where ω_s represents the network voltage vector's angular velocity.

4.1.2 Model simplification

Notice, that the sixth-order ODE model (4) is bilinear in its states and inputs because of the product terms (e.g.: $\delta_d i_{dc}$). As such, using design methods for linear systems is not straightforward. The high complexity given by the system's order is another problem to tackle. For designing classic MPC, linear, low-order equation systems are favorable. Hence simplification of the model would bring noteworthy benefits, making the MPC design more straightforward, when a linear system resulted. Since the AC and DC side's time constants differ significantly (as in the AC: $\omega_{ac} = \frac{1}{\sqrt{L_{ac}C_{ac}}} \cong 5.7 \cdot 10^3$ [rad/s], and on the DC: $\omega_{dc} = \frac{1}{\sqrt{L_{dc}C_{dc}}} \cong 2.8 \cdot 10^2$ [rad/s], see Table X. for reference). Thus, the differential equations can be separated into two sets, and the control of the AC and DC sides can be decoupled as described in [5]. The AC side model results as follows:

$$\begin{bmatrix} \dot{i}_{acd} \\ \dot{i}_{acq} \\ \dot{u}_{cd} \\ \dot{u}_{cq} \end{bmatrix} = \begin{bmatrix} -\frac{R}{L_{ac}} & \omega & -\frac{1}{L_{ac}} & 0 \\ -\omega & -\frac{R}{L_{ac}} & 0 & -\frac{1}{L_{ac}} \\ \frac{1}{C_{ac}} & 0 & 0 & \omega \\ 0 & \frac{1}{C_{ac}} & -\omega & 0 \end{bmatrix} \begin{bmatrix} i_{acd} \\ i_{acq} \\ u_{cd} \\ u_{cq} \end{bmatrix} + \begin{bmatrix} \frac{u_d}{L_{ac}} \\ \frac{u_q}{L_{ac}} \\ -\frac{\delta_d i_{dc}}{C_{ac}} \\ -\frac{\delta_q i_{dc}}{C_{ac}} \end{bmatrix} \quad (4.5)$$

Looking at the state matrix it can be further stated that there are only weak couplings between the d and q components. This allows to handle them separately, and later to design separate control for each. The equation system describing the DC side dynamics is the following:

$$\begin{bmatrix} \dot{i}_{dc} \\ \dot{u}_0 \end{bmatrix} = \begin{bmatrix} 0 & -\frac{1}{L_{dc}} \\ \frac{1}{C_{dc}} & -\frac{1}{R_{load}C_{dc}} \end{bmatrix} \begin{bmatrix} i_{dc} \\ u_0 \end{bmatrix} + \begin{bmatrix} \frac{1.5}{L_{dc}}(\delta_d u_{cd} + \delta_q u_{cq}) \\ 0 \end{bmatrix} \quad (4.6)$$

It can be noticed that, with the AC and DC model separation, bilinearity disappears, since the binding coefficients are present only in the input (\mathbf{u}) of the DC state space model. Consequently, all equations are linear and with a considerably lower order, making control design much easier and allowing for the application of linear design methods. For the DC side dynamics, the linear time invariant differential equation system's matrices can be identified for predictive control design purposes:

$$\begin{aligned} \mathbf{x} &= \begin{bmatrix} i_{dc} \\ u_0 \end{bmatrix}, \\ \mathbf{u} &= (\delta_d u_{cd} + \delta_q u_{cq}), \\ \mathbf{y} &= u_0, \\ \mathbf{A} &= \begin{bmatrix} 0 & -\frac{1}{L_{dc}} \\ \frac{1}{C_{dc}} & -\frac{1}{R_{load}C_{dc}} \end{bmatrix}, \\ \mathbf{B} &= \begin{bmatrix} i_{dc} \\ u_0 \end{bmatrix}, \\ \mathbf{C} &= \begin{bmatrix} 0 & 1 \end{bmatrix}. \end{aligned} \quad (4.7)$$

where \mathbf{x} , \mathbf{u} and \mathbf{y} are the state, input and output vectors of the DC-side system, and \mathbf{A} , \mathbf{B} and \mathbf{C} are the state, input and output matrices. The circuit

PARAMETER	VALUE
R	0.3ohm
Rload	10ohm
Lac	1mH
Ldc	30mH
Cac	30uF
Cdc	400uF
f	50Hz
fpwm	20kHz
Un	400V

Table 4.1: The applied parameters in model and controller design

parameters used for the implementation of the control structure based on this model are presented in Table 4.1.

4.1.3 Control structure

Relying on the possibility of separation of the AC-side and DC-side controllers, the control structure from Fig. 4.2. is proposed.

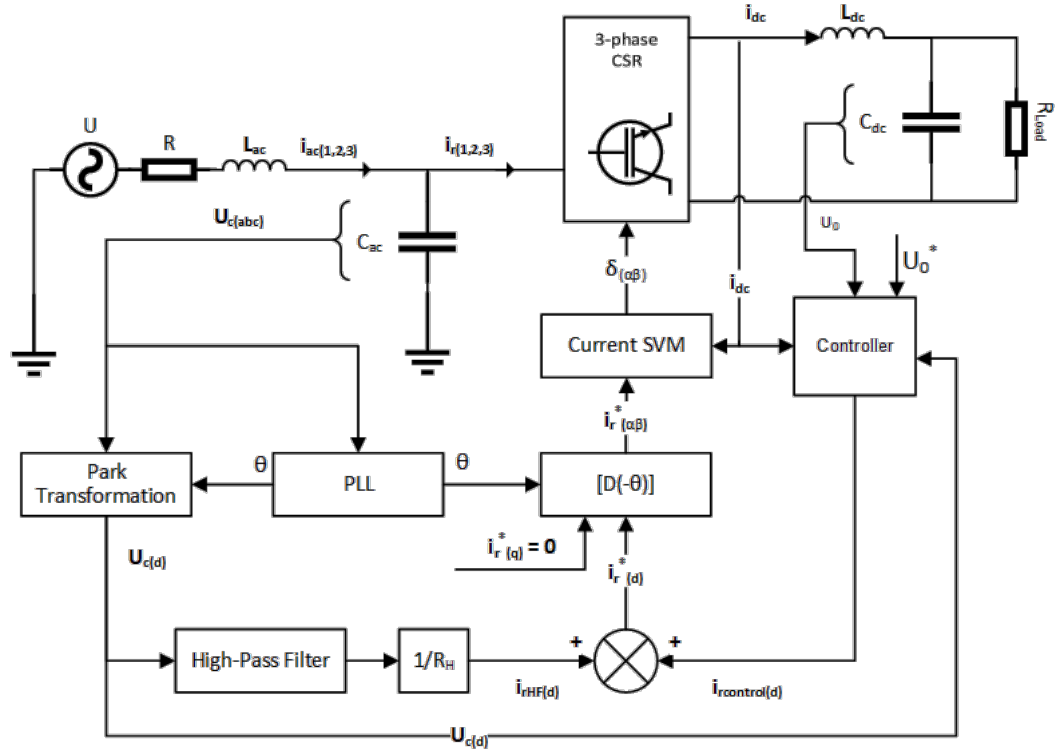


Figure 4.2: Block diagram of the control structure.

The controllers operate in the synchronous frame of the AC filter capacitor voltages $u_{c(1,2,3)}$, and the rectifier input currents $i_{r(1,2,3)}$ are in phase with the

capacitor voltages. The current reference $i_{\alpha\beta}^*$ supplied to the space vector modulation unit in the stationary frame, is obtained by coordinate transformation $[D(-\Theta)]$ of the current reference 4.8 delivered by the current controllers in the synchronous frame.

$$\begin{cases} i_{rd}^* = i_{rcontrol_d} + i_{rHF_d} \\ i_{rq}^* = 0 \end{cases} \quad (4.8)$$

In 4.8, $i_{rcontrol_d}$ represents the output of the DC voltage controller, while i_{rHF_d} represents the damping current, proportional with the high frequency component of the filter capacitor voltage (the fundamental component of the capacitor voltage in the stationary frame becomes a DC component in the synchronous frame). The DC and AC side control units are explained in more detail in the following sections, and the performance of the control structure is evaluated.

4.2 Control

write stuff here

4.2.1 DC-side explicit model predictive control

Model predictive control (MPC) is an efficient and systematic method for solving complex multi-variable constrained optimal control problems [86]. The basis can be examined in section 2.6, where the MPC control law is explained, namely, is based on the “receding horizon formulation”, where the model’s assumed behavior is calculated for a number of N steps, where N stands for the horizon’s length. Only the first step of the computed optimal input is applied in each iteration. The remaining steps of the optimal control input are discarded and a new optimal control problem (explained in chapter 2.6.2) is solved at the next sample time. Using this approach, the receding horizon policy provides the controller with the desired feedback characteristics, although with high order systems the computational effort is considerably demanding since all the steps should be taken in to account on the specified horizon in every iteration.

With Explicit MPC (EMPC), the discrete time constrained optimal control problem is reformulated as multi-parametric linear or quadratic programming. As explained in chapter 2.7, the problem of optimization can be solved offline, making it much more feasible from the perspective of the optimal control task. The optimum control law is a piecewise affine function of the states, and the resulting solution is stored in a pre-calculated lookup table. The parameter space, or the state-space is partitioned into critical regions. The real-time implementation consists in searching for the active critical region, where the measured state variables lie, and in applying the corresponding piecewise affine control law to achieve the desired dynamics. In order to introduce the MPC implementation from this paper, let us consider a linear discrete time system 4.9 derived with the discretisation of system 4.6 with zero-order hold method,

where control inputs are assumed piecewise constant over the simulation sample time $T_s = \frac{1}{f_s}$:

$$\begin{aligned} \mathbf{x}(t+1) &= \mathbf{A}_d \mathbf{x}(t) + \mathbf{B}_d \mathbf{u}(t) \\ \mathbf{y}(t) &= \mathbf{C}_d \mathbf{x}(t) \end{aligned} \quad (4.9)$$

where \mathbf{A}_d , \mathbf{B}_d , \mathbf{C}_d are the matrices of the discretised system derived from 4.7. With system 4.9 appears to be linear time invariant, MPC design can be followed. The following constraints have to be satisfied:

$$\begin{aligned} \mathbf{y}_{min} &\leq \mathbf{y}(t) \leq \mathbf{y}_{max}, \\ \mathbf{u}_{min} &\leq \mathbf{u}(t) \leq \mathbf{u}_{max} \end{aligned} \quad (4.10)$$

where $t > 0$, $\mathbf{x} \in \mathbb{R}^n$, $\mathbf{u} \in \mathbb{R}^m$, $\mathbf{y} \in \mathbb{R}^p$. The MPC solves the following constrained optimization problem [70]:

$$\min_{U=\{\mathbf{u}_t \dots \mathbf{u}_{t+N_u-1}\}} J(\mathbf{u}, \mathbf{x}(t)) = \sum_{k=0}^{N_y-1} (\mathbf{x}_{t+N_y|t}^T \mathbf{Q}_w \mathbf{x}_{t+N_y|t} + \mathbf{u}_{t+k}^T \mathbf{R}_w \mathbf{u}_{t+k}) \quad (4.11)$$

subject to:

$$\begin{aligned} \mathbf{x}_{min} &\leq \mathbf{x}_{t+k|t} \leq \mathbf{x}_{max}, \quad k = 1, \dots, N_c - 1 \\ \mathbf{u}_{min} &\leq \mathbf{u}_{t+k|t} \leq \mathbf{u}_{max}, \quad k = 1, \dots, N_c - 1 \\ \mathbf{x}_{t|t} &= \mathbf{x}(t), \quad \mathbf{u}_{t|t} = \mathbf{u}(t) \\ \mathbf{x}_{t+k+1|t} &= \mathbf{A}_d \mathbf{x}_{t+k|t} + \mathbf{B}_d \mathbf{u}_{t+k|t} \\ \mathbf{y}_{t+k|t} &= \mathbf{C}_d \mathbf{x}_{t+k|t} \\ \mathbf{u}_{t+k|t} &= -K \mathbf{x}_{t+k|t}, \quad k \geq 0 \end{aligned} \quad (4.12)$$

There the formulation of such problem is described in detail in chapter 2.6.2. This problem is solved at each time instant t , where $\mathbf{x}_{t+k|t}$ denotes the state vector predicted at time $t+k$, obtained by applying the input sequence $\mathbf{u}_{t|t} \dots \mathbf{u}_{t|t+1}$ to model 4.15, starting from the state $\mathbf{x}_{t|t}$. Further, it is assumed that Q and R , are symmetric positive semidefinite ($Q_w = Q_w^T \geq 0$, $R_w = R_w^T > 0$) and K is a feedback gain. Further, N_y, N_u, N_c are the output, input and constraint horizons, respectively. Using the model for predicting the future behavior of the system and with some appropriate substitution and variable manipulation, the problem 4.11,4.12 can be transformed to the standard multi parametric quadratic programming (mp-QP) form, as described in [70]:

$$V_z = \min \frac{1}{2} z^T H z \quad (4.13)$$

subject to:

$$Gz \leq W + S\mathbf{x}(t) \quad (4.14)$$

where the matrices H , G , W , S result directly from the coordinate transformations and variable manipulations. The solution of the mp-QP problem for each critical region has the form:

$$\mathbf{u}^* = f_i \mathbf{x} + g_i \quad (4.15)$$

and the critical region is described by:

$$\mathcal{C}_{reg_i} = \{\mathbf{x} \in R^n | H_i \mathbf{x} \leq K_i\} \quad (4.16)$$

Thus, the explicit MPC controller is completely characterized by the set of parameters:

$$\{f_i, g_i, H_i, K_i\}_{i=1 \dots N} \quad (4.17)$$

In case of the discrete time system resulting from 4.7, for sampling time equal with the switching period $T_s = 5 \cdot 10^{-5}$ s, the problem defined to be solved by MPC is the minimization of the quadratic cost function 4.9 for:

$$\mathbf{R}_w = \begin{bmatrix} 1 & 0 \\ 0 & 1 \end{bmatrix}, \mathbf{Q}_w = \begin{bmatrix} 10^{-6} & 0 \\ 0 & 10^{-6} \end{bmatrix}, N_y = N_u = N_c = 2 \quad (4.18)$$

Since N_y, N_u, N_c take the same value, they will be substituted by N . The constraints defined based on the rated power of the CSR $P_n = 2500$ W, are:

$$\begin{aligned} 0 &\leq i_{dc} \leq 50A \\ 0 &\leq u_0 \leq 500V \end{aligned} \quad (4.19)$$

The state space partition resulting from this problem has 13 critical regions, which can be observed in Fig. 4.3.

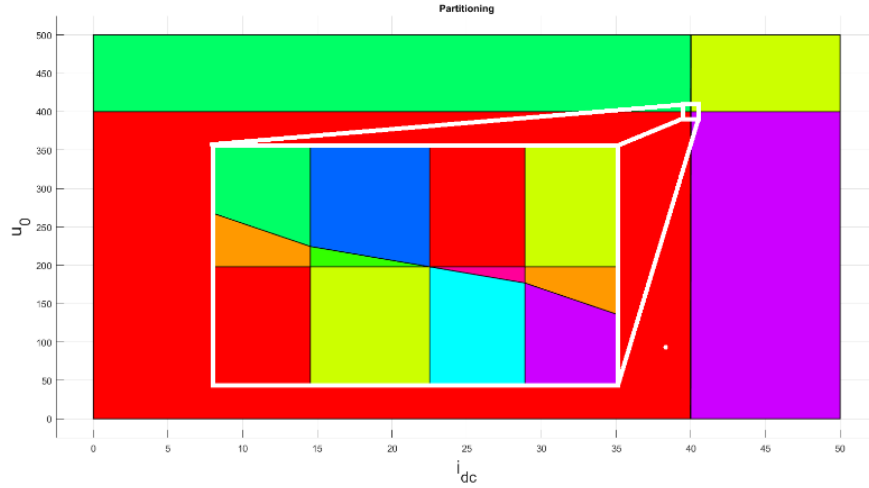


Figure 4.3: State space partitioning.

From the basis of the discredited model 4.9, the given constraints, and horizon 4.19 the cost function 4.11 is established via the MPT toolbox [30] and used in the generated controller for the EMPC design [29], [31]. The controller is created as a compliable S-function in the Matlab/Simulink environment and its place in the control structure can be observed in Fig. 4.4. as the EMPC controller. The output of the MPC controller is the control variable obtained via solving 4.12 and $u_{MPC} = (\delta_d u_{cd} + \delta_q u_{cq})$, from which the current reference

can be calculated using 4.19. The quadrature component u_{cq} is zero in the synchronous frame of the filter capacitor voltage.

$$\dot{i}_{rMPCd} = \frac{u_{MPC}}{u_{cd}} \cdot i_{dc} \quad (4.20)$$

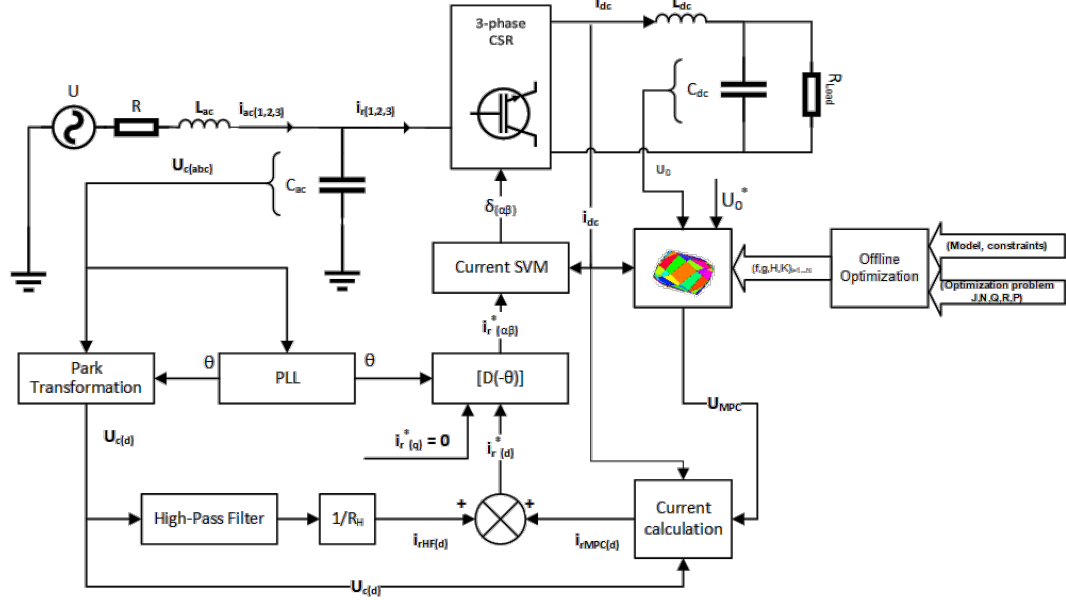


Figure 4.4: The control structure of the CSR, with MPC controller on the DC side.

4.2.2 Active AC-side damping

The CSR requires a voltage supply on the AC side. Taking into consideration the inductive character of the mains, the presence of a three-phase capacitor tank at the input of the CSR is a must. The most convenient is to use three-phase LC filtering with inductors on the lines and star connected capacitors resembling those in Fig. 4.1, although the resonance phenomena between these components can still cause difficult problems. The simplest way to dampen the resonance on the AC side LC filter is to add a damping resistor across the capacitor [69]. Because these resistors result in high losses, active damping methods have been proposed, which emulate damping resistors by control. This makes the CSR bridge produce an additional high frequency current, equivalent to the presence of virtual damping resistors connected in parallel with the AC capacitors. The resonance of the AC side LC filter produces harmonics in the capacitor voltage with frequency close to $\omega_{ac} = \frac{1}{\sqrt{L_{ac}C_{ac}}}$, which appears as $\omega_{ac} - \omega$ component in u_{cd} , where $\omega = 2\pi f$. The fundamental component of the capacitor voltage represents a DC component in the synchronous reference frame. Therefore, a high-pass filter (HPF) is applied to filter out this DC component, with the transfer function:

$$HPF(s) = \frac{s}{s + 0.1 \cdot (\omega_{ac} - \omega)} \quad (4.21)$$

A virtual damping resistance R_H has been defined for calculation of the damping current component i_{HPF} from the HPF component of the capacitor voltage.

4.3 Space vector modulation strategy

4.4 Modulation

The chosen modulation strategy is developed in the " $\alpha\beta$ " stationary reference frame, based on the notions already mentioned in section 2.4.1. The structure requires simultaneous conduction of the upper and lower transistors of the bridge, since the current of the L_{dc} choke must not be interrupted. Additionally, the switching devices are considered as ideal.

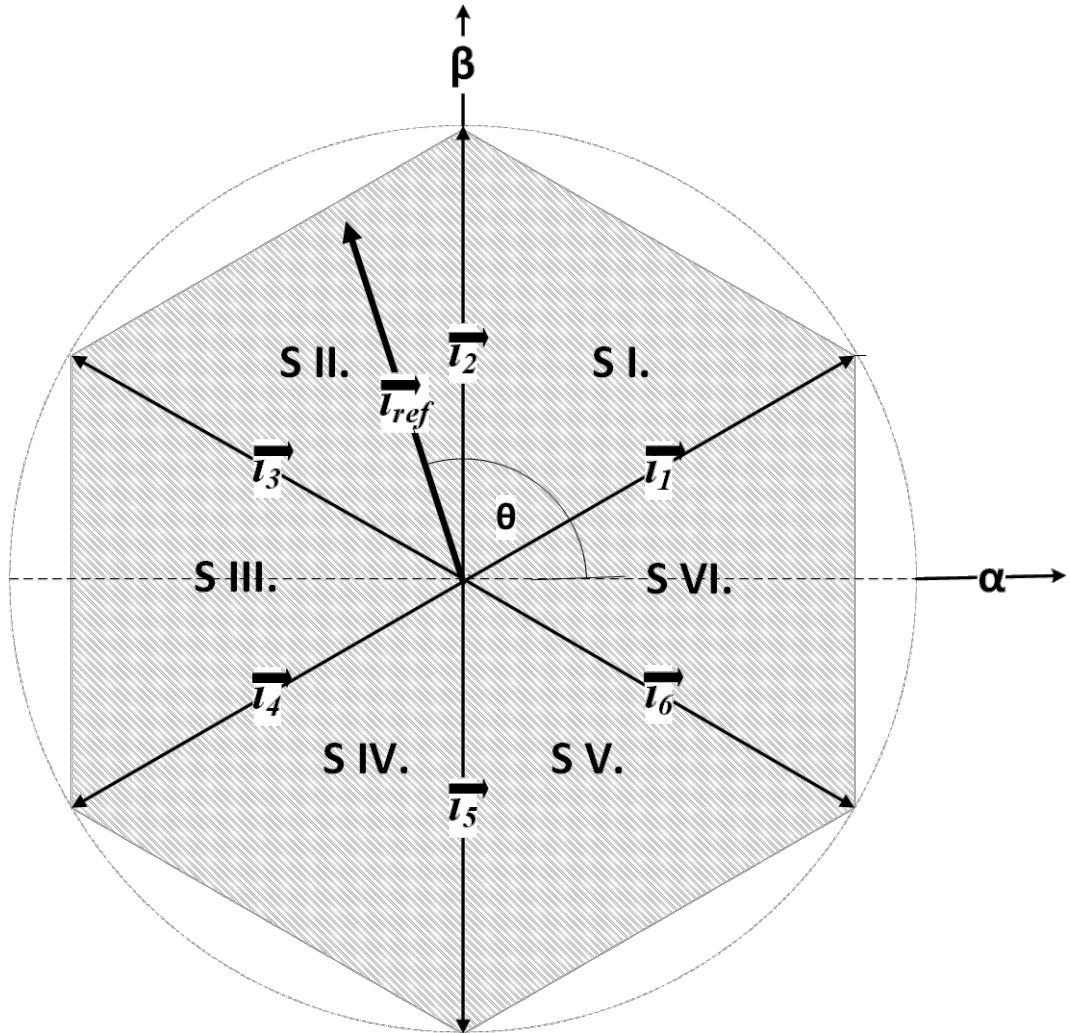


Figure 4.5: The fundamental input current vectors corresponding to the active switching states of the CSR.

According to this, one of the upper and one of the lower switches must be

Name	Switching State						Phase currents			Vector representation
	1	2	3	4	5	6	ia	ib	ic	
\vec{i}_1	1	0	0	0	0	1	i_{dc}	0	$-i_{dc}$	$2i_{dc}e^{j\pi/6}/\sqrt{3}$
\vec{i}_2	0	0	1	0	0	1	0	i_{dc}	$-i_{dc}$	$2i_{dc}e^{j\pi/2}/\sqrt{3}$
\vec{i}_3	0	1	1	0	0	0	$-i_{dc}$	i_{dc}	0	$2i_{dc}e^{j5\pi/6}/\sqrt{3}$
\vec{i}_4	0	1	0	0	1	0	$-i_{dc}$	0	i_{dc}	$2i_{dc}e^{j7\pi/6}/\sqrt{3}$
\vec{i}_5	0	0	0	1	1	0	0	$-i_{dc}$	i_{dc}	$2i_{dc}e^{j3\pi/2}/\sqrt{3}$
\vec{i}_6	1	0	0	1	0	0	i_{dc}	$-i_{dc}$	0	$2i_{dc}e^{j11\pi/6}/\sqrt{3}$
\vec{i}_7	1	1	0	0	0	0	0	0	0	0
\vec{i}_8	0	0	1	1	0	0	0	0	0	0
\vec{i}_9	0	0	0	0	1	1	0	0	0	0

Table 4.2: The fundamental input current vectors corresponding to the active switching states of the CSR.

closed at all times. This allows nine states, six of which are active. There are three "zero" vectors, corresponding to the switching states, when both devices of one of the bridge legs are in conduction. These current vectors are shown in Table 4.2.

The neighboring space phasors can be formulated as:

$$\begin{aligned}
 \vec{i}_n &= \frac{2}{\sqrt{3}}i_{dc}e^{j(\frac{n\pi}{3}-\frac{\pi}{6})} \\
 \vec{i}_{n+1} &= \frac{2}{\sqrt{3}}i_{dc}e^{j(\frac{n\pi}{3}+\frac{\pi}{6})} \\
 n &= 1, 2, \dots, 6
 \end{aligned} \tag{4.22}$$

The reference current vector is sampled with fixed sampling period T_s . The sampled value of \vec{i}_{ref} is synthesized as the time average of two neighbouring space phasors adjacent to the reference current:

$$T_n\vec{i}_n + T_{n+1}\vec{i}_{n+1} = T_s\vec{i}_{ref} \tag{4.23}$$

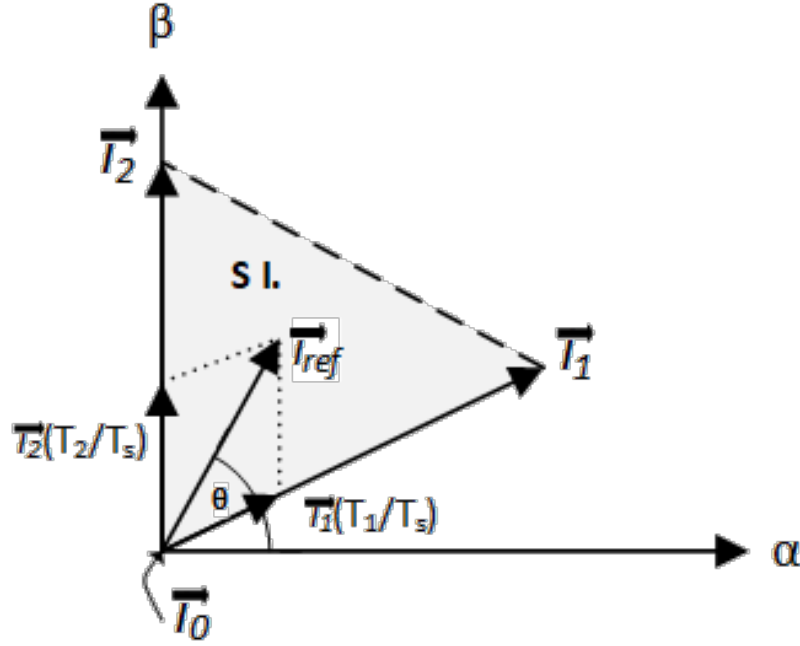
T_n and T_{n+1} represent the individual durations of the switching states corresponding to the neighboring vectors. For example, in case of a current reference vector situated in the first sector, T_1 , T_2 and T_0 can be calculated using 4.24.

$$\begin{aligned}
 T_1 &= T_s \frac{i_{ref\alpha}}{i_{dc}} \\
 T_2 &= T_s \frac{\sqrt{3}}{2i_{dc}} \left(i_{ref\beta} - \frac{i_{ref\alpha}}{\sqrt{3}} \right) \\
 t_0 &= T_s - T_n - T_{n-1} = T_{7,8,9}
 \end{aligned} \tag{4.24}$$

The complex plane is naturally divided by the fundamental space vectors into six areas, named "sectors".

$$\begin{aligned}
 x\frac{\pi}{6} + \frac{(n-1)\pi}{3} &\leq \theta_n \leq \frac{\pi}{6} + \frac{n\pi}{3} \\
 n &= 1, 2, \dots, 6
 \end{aligned} \tag{4.25}$$

The non-zero space vectors are selected based on the phase angle θ between \vec{i}_{ref} and the real axis. Table 4.3 presents an example of switching pattern in case of a current reference vector situated in Sector I.


 Figure 4.6: Synthesis of \vec{i}_{ref} by \vec{i}_1 , \vec{i}_2 , and \vec{i}_0

The switching scheme represented in Table 4.2. is aimed at reducing the number of commutations in a switching cycle, resulting in the reduction of the switching losses [57]. Additionally, the constraint (4.26) resulting from the available magnitudes of the current vectors, is applied to the current reference.

$$0 \leq |i_{ref}| \leq \frac{\sqrt{6}i_{dc}}{\cos\theta + \sqrt{3}\sin\theta} \quad (4.26)$$

	\vec{i}_1	\vec{i}_2	\vec{i}_0	\vec{i}_0	\vec{i}_2	\vec{i}_1
S1	1	1	1	1	1	1
S2	0	0	0	0	0	0
S3	1	1	0	0	1	1
S4	0	0	0	0	0	0
S5	1	1	0	0	1	1
S6	0	0	0	0	0	0
	T_s		\vdots		T_s	

Table 4.3: Representation of switching sequences for SECTOR I.

4.5 Discussion

From the continuous AC 4.5, and DC 4.6 model equations described in Ch.X., the controller is formulated from discretised system 4.9, and it is described via the cost function and control problem of 4.11, and 4.12 in Ch.X+1. The evaluated model and control structure are shown on Fig.4. In the following section said EMPC's computational requirements are evaluated, and the Matlab/Simulink simulation results are compared to a classic state feedback controller's dynamic performance.

4.5.1 Computational effort

The binary search tree generated for the control problem presented in Fig. 4.7. The search method and formulation of the tree is described in chapter 2.7.1. The depth of the search tree is 5 and it has a total number of 29 nodes. It is utilized with the MPT toolbox [58], [49], and it can be used for the computationally optimal real-time implementation of the proposed algorithm on low-cost hardware.

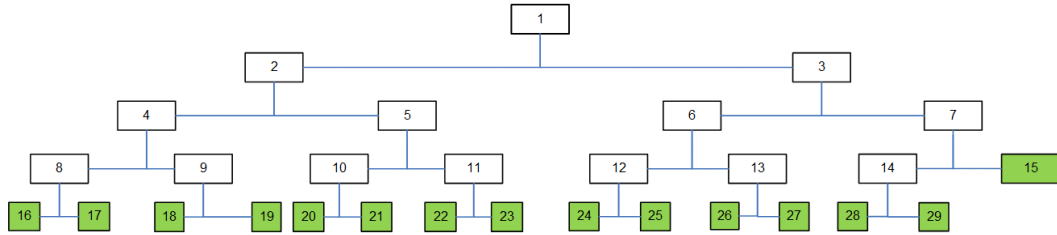


Figure 4.7: Binary search tree of the controller for a horizon of $N = 4$. The leaf nodes are depicted with filled squares. The depth of the tree is 5.

The search for an active critical region starts from the first level and represents the evaluation in each adjacent node of an inequality of the form: $x \leq K$. Thus, in this case a maximum number of 4 inequalities have to be evaluated to reach the active critical region. Implementing the presented algorithm is straightforward on a DSP processor, for instance from the dsPIC33 family by Microchip. Using the mac (multiply and accumulate) instruction the inequality is evaluated for each node using 4 instructions, thus in 80ns on a 50MIPS processor (Fig. 4.8). The active critical region can be reached in a maximum of 400ns. Compared to the typical sample rate of 10us in the case of a CSR, the real-time implementation on a DSP processor is possible.

4.5.2 Horizon performance

With the cost function (4.11) employed using (4.18), changing the length of the horizon (N) affects the system's complexity illustrated by the partition in the state space shown in Fig. 4.3., and Fig. 4.9 presents the step response of the controlled system for different lengths of the horizon. It shows, that the response is not affected by the increase of the horizon above $N = 2$, supporting the choice of this value for Matlab Simulink implementation.

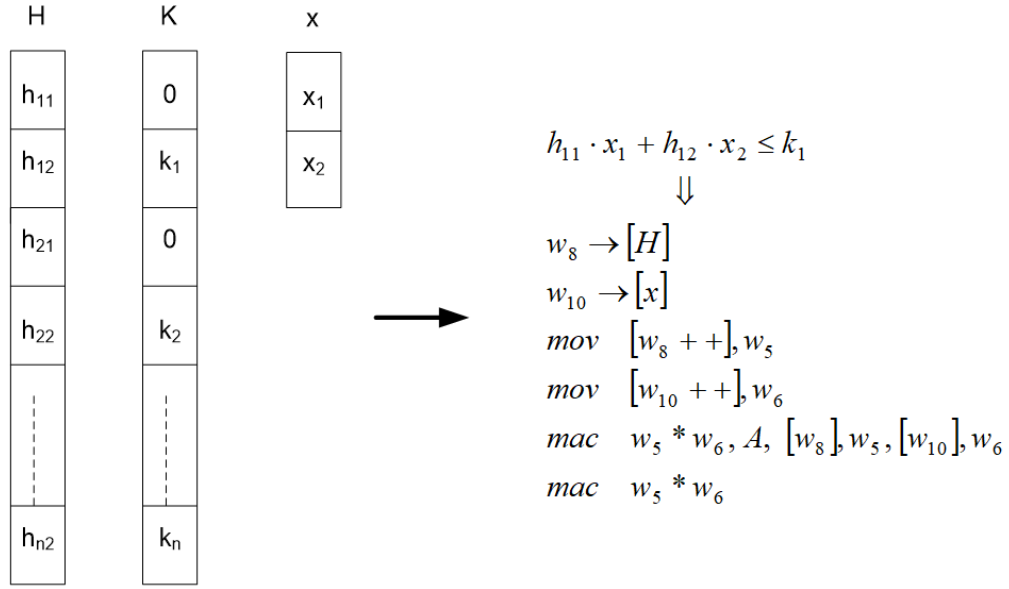


Figure 4.8: Data organization in the data memory of a single core DSP and the evaluation of a 2-dimensional inequality

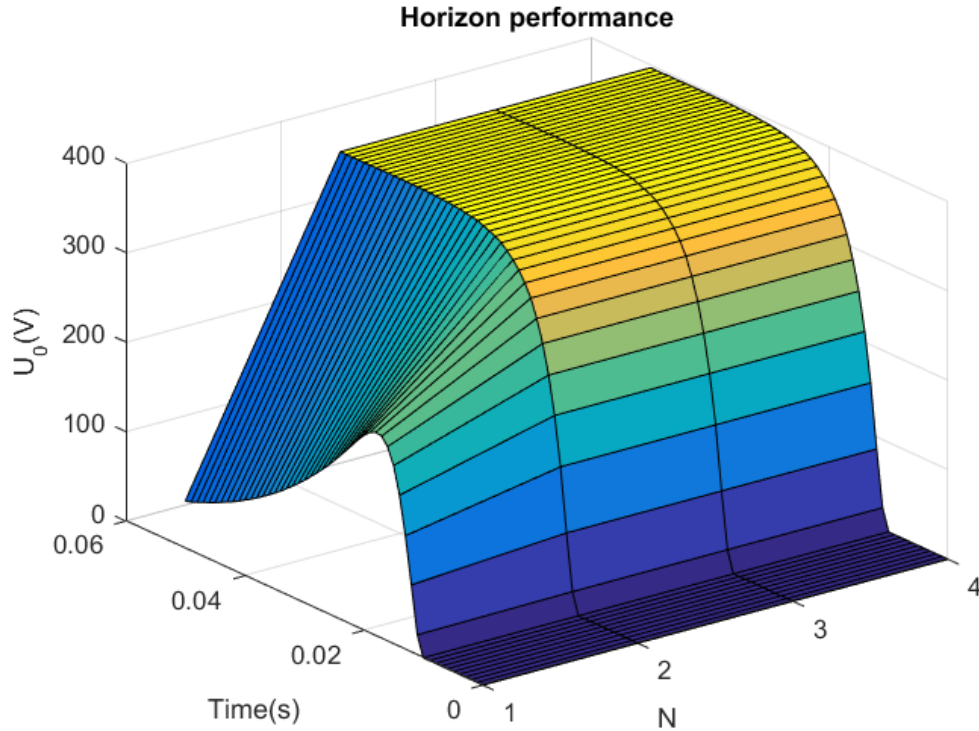


Figure 4.9: Step response of the system as a function of the horizon length (N).

4.5.3 Simulation results

The simulation results are produced with Matlab/Simulink. The discrete model's (4.9) simulation frequency was 1 MHz, with the model parameters

represented in Table 4.1., and with the control structure shown on Fig. 4.2. The EMPC performance is shown below:

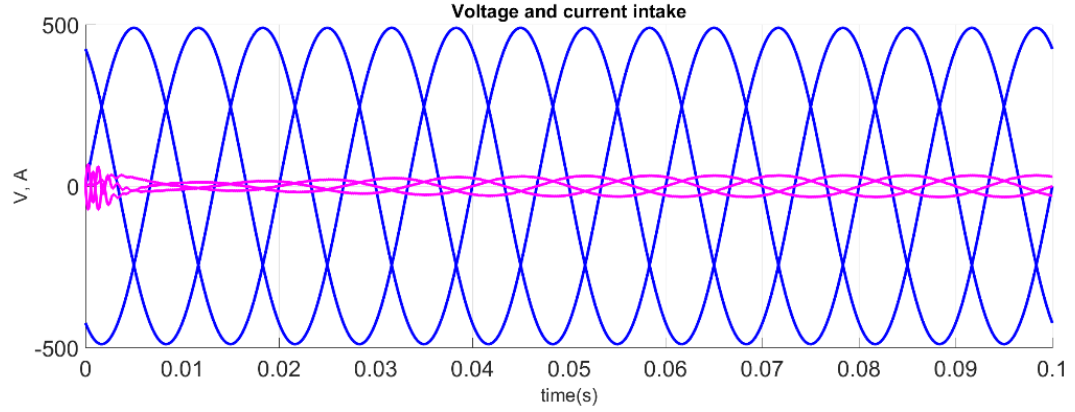


Figure 4.10: Three-phase voltage and current intake of the CSR with EMPC

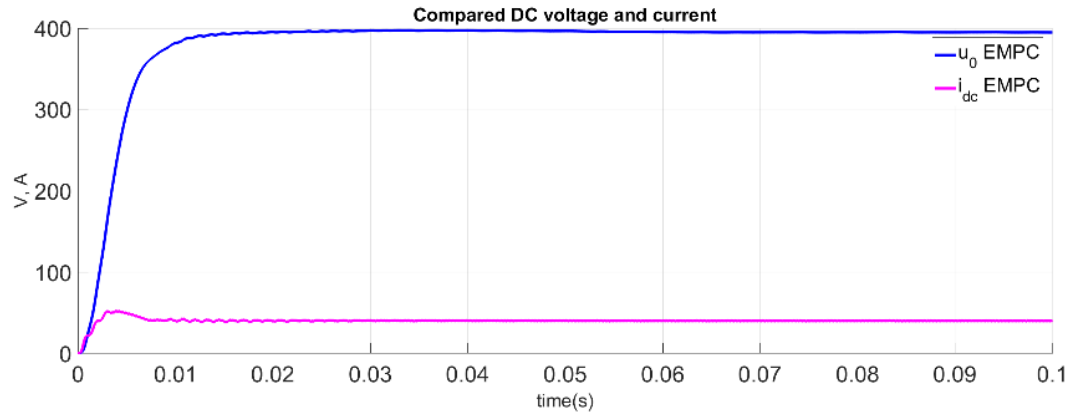


Figure 4.11: Resulting current and voltage trajectories of the CSR with (EMPC).

More details about the Matlab simulation are presented in [62].

4.5.4 Comparison with a state feedback control

On the DC side, not only the output voltage u_0 but also the inductor current i_{dc} needs to be controlled. Described in [28], a state feedback control with optimal parameters can be used as a reference based on the model properties listed in Table 4.1, with output voltage u_0 and DC bus current i_{dc} chosen as

the state variables. Since u_0 is a DC quantity in steady state, an integrator signal is introduced to diminish the steady-state error. The structure of the controller is represented in Fig. 4.12.

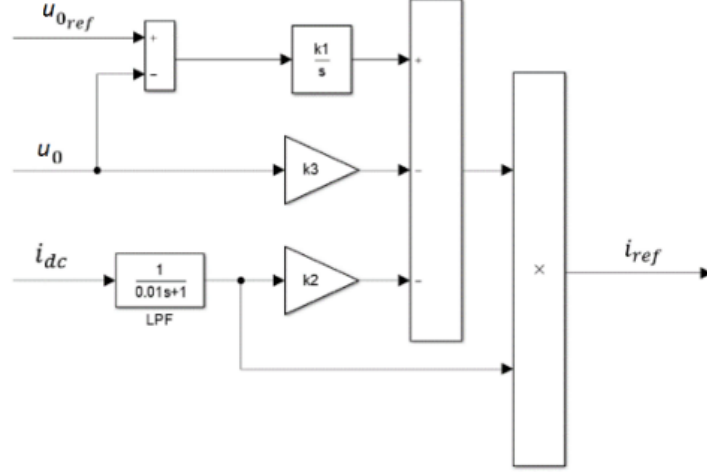


Figure 4.12: Simple DC side state feedback control structure.

The tuning constants applied and calculated according to [29] are:

$$\begin{aligned} k1 &= \frac{\omega_n^3}{1.5U_n\omega_{dc}^2}, k2 = \frac{1.9\omega_n L_{dc}}{1.5U_n}, k3 = \frac{2.2\omega_n^2}{1.5U_n(\omega_{dc}^2-1)}, \\ \text{where,} \\ \omega_n &= 1.1, \omega_{ac} = \frac{1}{\sqrt{L_{ac}C_{ac}}}, \omega_{dc} = \frac{1}{\sqrt{L_{dc}C_{dc}}} \end{aligned} \quad (4.27)$$

The state feedback controllers block on the diagram is taking the controller's place, shown on Fig. 4.2. The independent outputs are the high pass filter's output $i_{rHPF(d)}$ and the controller's output $i_{rcontrol(d)}$. The sum of the independent current values is converted to Clarke frame to be able to govern the switching states of the IGBT's. This can be done because $i_{rHF(d)}$ has only high frequency components and $i_{rcontrol(d)}$ has low frequency components due to the differences in LC time constants, as discussed in the second section. Then the control signal governing the switches is applied in the same manner, described at the start of section 4.4. The state feedback control's performance in comparison with the EMPC is shown in Fig. 4.13.

4.6 Conclusion

The constrained, model-based optimal control of a current source rectifier has been presented in this paper. The dynamic model of a three-phase current source rectifier has been developed in Park frame. The proposed model has been examined from the design and implementation points of view with the purpose of explicit model-based predictive control. It proved to be the case that the regular set of differential equations of the CSR appears to be too complex, and contains non-linearity for such a design approach. To address this issue the usage of separated AC and DC equation sets was suggested to avoid

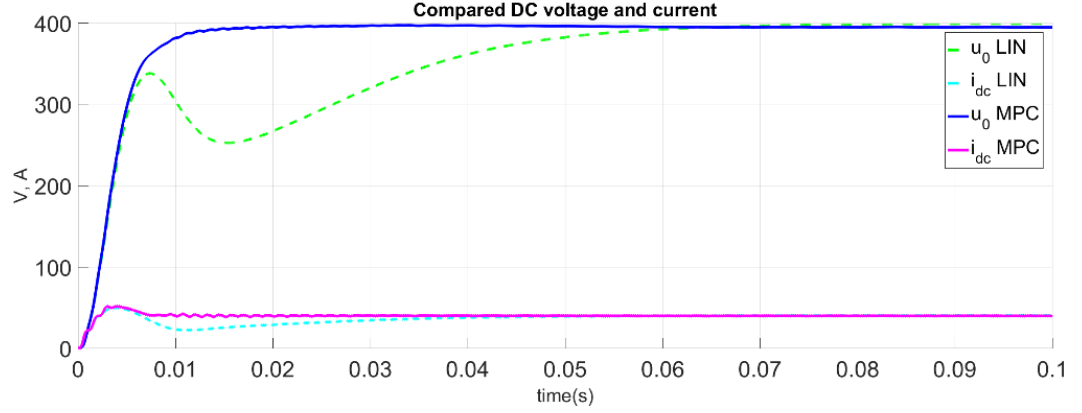


Figure 4.13: Resulting current and voltage trajectories of the CSR with explicit model predictive control (MPC) compared state feedback control (LIN).

linearization and complexity reduction. This solution eliminates bilinearity and enables the application of linear control design techniques. Current-based SVPWM of the three-phase converter has been used with an emphasis on the reduction of switching losses. Throughout the article the explicit model predictive control method is described and the method's effectiveness compared to conventional state feedback control is shown. The implementation and simulation experiments have been performed in Matlab/Simulink environment. Moreover, the proper implementation of the system in a modern DSP chip will result in real-time operation.

Chapter 5

Summary

5.1 Thesis: Constrained, explicit predictive control for current source buck-type rectifiers

I proposed a simplified CSR model, which was derived from the well known CSR structure and was examined from design and implementation points of view with the purpose of explicit model-based predictive control. The regular set of differential equations of the CSR appeared to be too complex for my a design approach, for applying explicit predictive control. I adressed this issue with the separation AC and DC equation sets was of the CSR to decrease complexity and easy controller design. With this solution I eliminated bilinearity and enabled the application of linear control design techniques. I used current-based SVPWM the modulation, what has been used with an emphasis on the reduction of switching losses. For DC side control I implemented explicit model predictive control (EMPC) and I compared this method's effectiveness to conventional state feedback control (SFC). I implemented the CSR structure and the proposed controller with EMPC on DC and active damping on the AC side in Matlab/Simulink environment and tested by simulation. Additionally, I tested the proper implementation's computational requirements in a modern DSP chip, which would serve in real-time operation.

5.2 Thesis: Geometrical indicator for voltage unbalance in three phase networks

I extended the currently used measures of voltage unbalance with a new norm candidate. I found out that it is more demanding from the computational point of view, but has a new feature namely it checks electrical asymmetry, i.e. the norm of a ± 120 degree rotated version of the ideal three phase phasor is zero in the geometrical sense. I compared my geometrical approach to the standard wide-spread use of voltage unbalance indicator (TDV) and found out it carries additional information, whilst retaining it's original purpose.

5.3 Thesis: Voltage unbalance compensation with optimization based control algorithm and asymmetrical inverter structure

I found out that the regular current controlling applications would not fit to the purpose for reducing voltage unbalance whilst only relying on the voltage measurement. As such I developed an asymmetrical current source inverter (ACSI) circuit with combined asynchronous parallel pattern search (APPS) control structure, in Matlab/Simulink environment, and I applied the my geometrical norm as a cost function. I showed with validating simulations, that the geometrical based unbalance indicator can serve as a basis of further research. The fundamental element of the system is a modified three phase inverter that is capable of the asymmetric injection of any current waveforms to the network. The optimization based control algorithm injects the available energy (as current waveform) in such a way, that the voltage unbalance decreases. This optimization problem is usually constrained by the available renewable energy supplied by the power plant. This suggested controller with combined ACSI structure enables the residential users owning a grid synchronized domestic power plant to reduce voltage unbalance measurable at any low voltage domestic the connection point. I also tested the control structure on a real low voltage network model in a dynamical simulation environment consisting of the models of the electrical grid, a domestic power plant, ACSI, and different types of loads. Different simulation experiments has been run for each norm and for both the power constrained and unconstrained case. I showed with the evaluation that this structure can serve as a residential level voltage quality improvement method for the three phase low voltage network.

List of notations

Chapter 4.1. notations

\mathbf{A}	State matrix of the DC side system
\mathbf{A}_d	Discretised state matrix of the DC side system
\mathbf{B}	Input matrix of the DC side system
\mathbf{B}_d	Discretised input matrix of the DC side system
C_{ac}	AC side inductance
C_{dc}	DC side inductance
\mathbf{C}	Output matrix of the DC side system
\mathbf{C}_d	Discretised output matrix of the DC side system
C_{reg_i}	Critical region
$D(-\Theta)$	Inverse Clarke transformation
f	Network voltage frequency
f_{pwm}	Rectifier switching frequency
f_s	Simulation frequency
f_i	?
g_i	?
G	?
H	?
$HPF(s)$	High pass filter transfer function
$i_{ac1,2,3}$	AC side inductance current
$i_{ac\alpha,\beta}$	AC side inductance current in Clarke frame
$i_{acd,q}$	AC side inductance current in Park frame
i_{HPF}	AC side damping current
$i_{r1,2,3}$	Rectifier current
i_{rMPC_d}	Direct component of the output of the EMPC controller
$i_{r1,2,3}^*$	Rectifier reference current
$i_{r\alpha,\beta}^*$	Rectifier reference current in Clarke frame
$i_{rcontrol_d}$	Direct component of the output of the DC voltage controller
i_{rHF_d}	Direct component of the damping current of AC noise
i_{dc}	DC side inductance current
$i_{ref\alpha,\beta}$	α , or β component of the reference current vector respectively
$\vec{i}_{0,\dots,9}$	Current vector of the phasor
\vec{i}_{ref}	Reference current vector
J	Quadratic EMPC cost function
$k_{1,2,3}$	State feedback controller's coefficients
K	Feedback gain of EMPC controller

L_{ac}	AC side inductance
L_{dc}	DC side inductance
n	Current phasor sector indicator
N	Control horizon
N_y, N_u, N_c	Output, input and constraint horizons
P_n	Nominal power of the CRS
\mathbf{Q}_w	State weight matrix of quadratic MPC cost function
R	Phase resistance
R_H	Virtual damping resistance
R_{load}	Load resistance
\mathbf{R}_w	Input weight matrix of quadratic MPC cost function
\mathbb{R}	Set of real numbers
S	Current phasor sector
\mathbf{S}	?
t	Discrete timestep
T_s	Switching period
$T_{0,...,9}$	Dwell time in the corresponding sector
\mathbf{u}	Output vector of the DC side system
$u_{1,2,3}$	AC side phase voltage
$u_{\alpha,\beta}$	AC side phase voltage in Clarke frame
$u_{d,q}$	AC side phase voltage in Park frame
$u_{c1,2,3}$	AC side capacitance voltage
$u_{c\alpha,\beta}$	AC side capacitance voltage in Clarke frame
$u_{cd,q}$	AC side capacitance voltage in Park frame
u_0	DC side voltage on load
u_0^*	DC side voltage reference
u_{MPC}	MPC control variable
\mathbf{u}^*	?
U	Set of MPC inputs
Un	Network line-to-line voltage
\mathbf{x}	State vector of the DC side system
\mathbf{y}	Input vector of the DC side system
V_z	?
$\delta_{1,2,3}$	Conduction state leg in Clarke frame
$\delta_{\alpha,\beta}$	Conduction state leg in Park frame
$\delta_{d,q}$	Conduction state leg
θ	Network voltage vector's angular displacement
ω	Network voltage vector's angular velocity
ω_{ac}	Ac side LC filter angular velocity
ω_n	Damping angular velocity

Chapter 4.2. notations

$IEEEv_{936}$?
$IEEEv_{112}$?
V_{an}, V_{bn}, V_{cn}	Line-to-neutral network voltage
V_{ab}, V_{bc}, V_{ca}	Line-to-line network voltage
MDV	?

5.3. THESIS: VOLTAGE UNBALANCE COMPENSATION WITH
OPTIMIZATION BASED CONTROL ALGORITHM AND
ASYMMETRICAL INVERTER STRUCTURE CHAPTER 5. SUMMARY

VUF	Voltage unbalance factor
$V_{1,...,n}$	Voltage of the n^{th} harmonic
ΔR	Vectorial deviation of the R^{th} phase
ΔS	Vectorial deviation of the S^{th} phase
ΔT	Vectorial deviation of the T^{th} phase
N	Vectorial voltage deviation from the balanced state
G	Geometrical voltage deviation from the balanced state
Δ_{Ideal}	Triangle of Ideal voltage vectors
Δ_{Real}	Triangle of real voltage vectors
<hr/>	
Chapter 4.3. notations	
x^k	Local multivariate extreme state at the k^{th} timestep
t_k	Timestep at the k
k	Discrete timestep
Δ_k	?
d_i	?
D	?
p	?
P_{loss}	Lost power per household due to network unbalance
P_{loss}^{comp}	Assumed network loss with unbalance compensation control
ΔP_{loss}	Saved power with unbalance compensation control
<hr/>	

Abbreviations

AC:	Alternating current
DC:	Direct current
VSR:	Voltage source rectifier
CSR:	Current source rectifier
MPC:	Model predictive control
MPT:	Model predictive control toolbox
EMPC:	Explicit model predictive control
HPF:	High pass filter
SVPWM	Space vector pulse width modulated
SFC:	State feedback control
MDV:	?
MIMO	Multiple input, multiple output
VUF:	Voltage unbalance factor (i.e. TDV)
CVUF:	Complex voltage unbalance factor
THD:	Total harmonic distortion
IGBT:	Insulated gate bipolar transistor
MPPT:	Maximum power point tracking
ACSI:	Asymmetrical current source inverter
TPWM:	Trapezoidal pulse width modulation
SVM:	Space vector modulation
SHE:	Selective harmonic elimination

Appendix

Stuff that is less relevant.

Bibliography

- [1] Ieee recommended practice for electric power distribution for industrial plants (ieee red book). pages 1–609, Oct 1986.
- [2] Ieee guide for self-commutated converters. pages 0_1–, 1987.
- [3] Ieee standard for inverse-time characteristics equations for overcurrent relays. pages 1–25, Feb 2019.
- [4] M. Hackl Statistical data of the hungarian electricity system. *Mavir Hungarian Independent Transmission Operator Company, Ltd.*, pages 899–906, 2011.
- [5] Syed Faiz Ahmed, Ch Fahad Azim, Hazry Desa, and Abadal-Salam T Hussain. Model predictive controller-based single phase pulse width modulation (pwm) inverter for ups systems. *Acta Polytechnica Hungarica*, 11(6):23–38, 2014.
- [6] Leandro Ramos Araujo, DRR Penido, Sandoval Carneiro, and José Luiz R Pereira. A three-phase optimal power-flow algorithm to mitigate voltage unbalance. *IEEE Transactions on Power Delivery*, 28(4):2394–2402, 2013.
- [7] Stefan Arnborg, Göran Andersson, David J Hill, and Ian A Hiskens. On undervoltage load shedding in power systems. *International Journal of Electrical Power & Energy Systems*, 19(2):141–149, 1997.
- [8] Yavuz Ates, Mehmet Uzunoglu, Arif Karakas, Ali Rifat Boynuegri, Abdullah Nadar, and Bulent Dag. Implementation of adaptive relay coordination in distribution systems including distributed generation. *Journal of cleaner production*, 112:2697–2705, 2016.
- [9] Martina Baumann, Uwe Drofenik, and Johann W Kolar. New wide input voltage range three-phase unity power factor rectifier formed by integration of a three-switch buck-derived front-end and a dc/dc boost converter output stage. In *INTELEC. Twenty-Second International Telecommunications Energy Conference (Cat. No. 00CH37131)*, pages 461–470. IEEE, 2000.
- [10] Martina Baumann and Johann W Kolar. A novel control concept for reliable operation of a three-phase three-switch buck-type unity-power-factor rectifier with integrated boost output stage under heavily unbalanced

- mains condition. *IEEE Transactions on Industrial Electronics*, 52(2):399–409, 2005.
- [11] RE Betz, T Summers, T Furney, et al. Symmetry compensation using a h-bridge multilevel statcom with zero sequence injection. In *Industry Applications Conference, 2006. 41st IAS Annual Meeting. Conference Record of the 2006 IEEE*, volume 4, pages 1724–1731, 2006.
 - [12] M Tavakoli Bina and A Kashefi. Three-phase unbalance of distribution systems: Complementary analysis and experimental case study. *International Journal of Electrical Power & Energy Systems*, 33(4):817–826, 2011.
 - [13] Austin H Bonnett and GC Soukup. Understanding the nema motor-generator standards of section mg-1-1993, revision 3, three-phase induction motors. In *Record of Conference Papers. IEEE Industry Applications Society 44th Annual Petroleum and Chemical Industry Conference*, pages 225–238. IEEE, 1997.
 - [14] Francesco Borrelli, Alberto Bemporad, and Manfred Morari. *Predictive control for linear and hybrid systems*. Cambridge University Press, 2017.
 - [15] Ted Brekken, Ned Mohan, and Tore Undeland. Control of a doubly-fed induction wind generator under unbalanced grid voltage conditions. In *2005 European Conference on Power Electronics and Applications*, pages 10–pp. IEEE, 2005.
 - [16] Amitava Chatterjee, Ranajit Chatterjee, Fumitoshi Matsuno, and Takahiro Endo. Augmented stable fuzzy control for flexible robotic arm using lmi approach and neuro-fuzzy state space modeling. *IEEE transactions on industrial electronics*, 55(3):1256–1270, 2008.
 - [17] M’hamed Chebre, Abdelkader Meroufel, and Yessema Bendaha. Speed control of induction motor using genetic algorithm-based pi controller. *Acta Polytechnica Hungarica*, 8(6):141–153, 2011.
 - [18] Daolian Chen, Jiahui Jiang, Yanhui Qiu, Jie Zhang, and Fusong Huang. Single-stage three-phase current-source photovoltaic grid-connected inverter high voltage transmission ratio. *IEEE Transactions on Power Electronics*, 32(10):7591–7601, 2016.
 - [19] Tsai-Hsiang Chen, Cheng-Han Yang, and Nien-Che Yang. Examination of the definitions of voltage unbalance. *International Journal of Electrical Power & Energy Systems*, 49:380–385, 2013.
 - [20] Federica Cucchiella, Idiano D’Adamo, and SC Lenny Koh. Environmental and economic analysis of building integrated photovoltaic systems in italian regions. *Journal of Cleaner Production*, 98:241–252, 2015.

- [21] Roger C Dugan, Mark F McGranaghan, and H Wayne Beaty. Electrical power systems quality. *New York, NY: McGraw-Hill, c1996*, 1996.
- [22] C Eugene. A new simple and effective approximate formulation for determination of three-phase unbalance by the voltmeter method. In *CIGRE 1986*, page 11, 1986.
- [23] Bruno Exposto, Rui Rodrigues, JG Pinto, Vítor Monteiro, Delfim Pedrosa, and João L Afonso. Predictive control of a current-source inverter for solar photovoltaic grid interface. In *2015 9th International Conference on Compatibility and Power Electronics (CPE)*, pages 113–118. IEEE, 2015.
- [24] Hamza Feroura, Fateh Krim, Billel Tabli, and Abdelbaset Laib. Finite-set model predictive voltage control for islanded three phase current source inverter. In *2017 5th International Conference on Electrical Engineering-Boumerdes (ICEE-B)*, pages 1–5. IEEE, 2017.
- [25] Charles L Fortescue. Method of symmetrical co-ordinates applied to the solution of polyphase networks. *Transactions of the American Institute of Electrical Engineers*, 37(2):1027–1140, 1918.
- [26] Hang Gao, Dewei Xu, Bin Wu, and Navid R Zargari. Model predictive control for five-level current source converter with dc current balancing capability. In *IECON 2017-43rd Annual Conference of the IEEE Industrial Electronics Society*, pages 8230–8235. IEEE, 2017.
- [27] Bachir Ghalem and Bendiabdellah Azeddine. Six-phase matrix converter fed double star induction motor. *Acta Polytechnica Hungarica*, 7(3):163–176, 2010.
- [28] Piotr Gnaciński, Marcin Pepliński, Damian Hallmann, and Piotr Jankowski. Induction cage machine thermal transients under lowered voltage quality. *IET Electric Power Applications*, 13(4):479–486, 2019.
- [29] Agata Godlewska and Andrzej Sikorski. Predictive control of current source rectifier. In *2015 Selected Problems of Electrical Engineering and Electronics (WZEE)*, pages 1–6. IEEE, 2015.
- [30] Peter Görbe, Attila Fodor, Attila Magyar, and Katalin M Hangos. Experimental study of the nonlinear distortion caused by domestic power plants. *Applied Thermal Engineering*, 70(2):1288–1293, 2014.
- [31] Péter Görbe, Attila Magyar, and Katalin M Hangos. Reduction of power losses with smart grids fueled with renewable sources and applying ev batteries. *Journal of cleaner production*, 34:125–137, 2012.
- [32] Xiaoqiang Guo, Yong Yang, and Xue Zhang. Advanced control of grid-connected current source converter under unbalanced grid voltage conditions. *IEEE Transactions on Industrial Electronics*, 65(12):9225–9233, 2018.

- [33] Sandeep Gupta and Ramesh Kumar Tripathi. Two-area power system stability improvement using a robust controller-based csc-statcom. *Acta Polytechnica Hungarica*, 11(7):135–155, 2014.
- [34] Tamás Haidegger, Levente Kovács, Radu-Emil Precup, Balázs Benyó, Zoltán Benyó, and Stefan Preitl. Simulation and control for telerobots in space medicine. *Acta Astronautica*, 81(1):390–402, 2012.
- [35] Yang Han, Lin Xu, Muhammad Mansoor Khan, and Chen Chen. Control strategies, robustness analysis, digital simulation and practical implementation for a hybrid apf with a resonant ac-link. *Acta polytechnica hungarica*, 7(5), 2010.
- [36] Jun Hang, Jianzhong Zhang, Ming Cheng, and Jin Huang. Online interturn fault diagnosis of permanent magnet synchronous machine using zero-sequence components. *IEEE Transactions on Power Electronics*, 30(12):6731–6741, 2015.
- [37] Roger A Horn and Charles R Johnson. *Matrix analysis*. Cambridge university press, 2012.
- [38] Patricia D Hough, Tamara G Kolda, and Virginia J Torczon. Asynchronous parallel pattern search for nonlinear optimization. *SIAM Journal on Scientific Computing*, 23(1):134–156, 2001.
- [39] Junjie Hu, Mattia Marinelli, Massimiliano Coppo, Antonio Zecchino, and Henrik W Bindner. Coordinated voltage control of a decoupled three-phase on-load tap changer transformer and photovoltaic inverters for managing unbalanced networks. *Electric Power Systems Research*, 131:264–274, 2016.
- [40] Shigenori Inoue and Hirofumi Akagi. A bidirectional dc–dc converter for an energy storage system with galvanic isolation. *IEEE Transactions on Power Electronics*, 22(6):2299–2306, 2007.
- [41] R Itoh. Steady-state and transient characteristics of a single-way step-down pwm gto voltage-source convertor with sinusoidal supply currents. In *IEE Proceedings B (Electric Power Applications)*, volume 136, pages 168–175. IET, 1989.
- [42] JK Kaldellis, M Simotas, D Zafirakis, and E Kondili. Optimum autonomous photovoltaic solution for the greek islands on the basis of energy pay-back analysis. *Journal of Cleaner Production*, 17(15):1311–1323, 2009.
- [43] András Kelemen, Nimród Kutasi, Mária Imecs, and Ioan Iov Incze. Constrained optimal direct power control of voltage-source pwm rectifiers. In *2010 IEEE 14th International Conference on Intelligent Engineering Systems*, pages 249–254. IEEE, 2010.

- [44] MN Kheraluwala, Randal W Gascoigne, Deepakraj M Divan, and Eric D Baumann. Performance characterization of a high-power dual active bridge dc-to-dc converter. *IEEE Transactions on industry applications*, 28(6):1294–1301, 1992.
- [45] P Giridhar Kini, Ramesh C Bansal, and Radhakrishna S Aithal. A novel approach toward interpretation and application of voltage unbalance factor. *IEEE transactions on industrial electronics*, 54(4):2315–2322, 2007.
- [46] Johann W Kolar, Hans Ertl, and Franz C Zach. Design and experimental investigation of a three-phase high power density high efficiency unity power factor pwm (vienna) rectifier employing a novel integrated power semiconductor module. In *Proceedings of Applied Power Electronics Conference. APEC'96*, volume 2, pages 514–523. IEEE, 1996.
- [47] Tamara G Kolda and Virginia J Torczon. Understanding asynchronous parallel pattern search. In *High Performance Algorithms and Software for Nonlinear Optimization*, pages 323–342. Springer, 2003.
- [48] NV Korovkin, QS Vu, and RA Yazenin. A method for minimization of unbalanced mode in three-phase power systems. In *2016 IEEE NW Russia Young Researchers in Electrical and Electronic Engineering Conference (EIconRusNW)*, pages 611–614. IEEE, 2016.
- [49] Nimród Kutasi, András Kelemen, and Mária Imecs. Constrained optimal control of three-phase ac-dc boost converters. In *2010 IEEE International Conference on Automation, Quality and Testing, Robotics (AQTR)*, volume 1, pages 1–6. IEEE, 2010.
- [50] Ching-Yin Lee, Bin-Kwie Chen, Wei-Jen Lee, and Yen-Feng Hsu. Effects of various unbalanced voltages on the operation performance of an induction motor under the same voltage unbalance factor condition. *Electric Power Systems Research*, 47(3):153–163, 1998.
- [51] Kevin Lee, Thomas M Jahns, Thomas A Lipo, and Vladimir Blasko. New control method including state observer of voltage unbalance for grid voltage-source converters. *IEEE Transactions on Industrial Electronics*, 57(6):2054–2065, 2009.
- [52] Yunwei Li, D Mahinda Vilathgamuwa, and Poh Chiang Loh. Microgrid power quality enhancement using a three-phase four-wire grid-interfacing compensator. *IEEE transactions on industry applications*, 41(6):1707–1719, 2005.
- [53] Peter D Lund, Jani Mikkola, and J Ypyä. Smart energy system design for large clean power schemes in urban areas. *Journal of Cleaner Production*, 103:437–445, 2015.

- [54] Luigi Malesani and Paolo Tenti. Three-phase ac/dc pwm converter with sinusoidal ac currents and minimum filter requirements. *IEEE Transactions on Industry Applications*, (1):71–77, 1987.
- [55] Aranzazu D Martin, Reyes S Herrera, Jesus R Vazquez, Paul Crolla, and Graeme M Burt. Unbalance and harmonic distortion assessment in an experimental distribution network. *Electric Power Systems Research*, 127:271–279, 2015.
- [56] Bart Meersman, Bert Renders, Lieven Degroote, Tine Vandoorn, and Lieven Vandevelde. Three-phase inverter-connected dg-units and voltage unbalance. *Electric Power Systems Research*, 81(4):899–906, 2011.
- [57] Leila Moussaoui and Ammar Moussi. An open loop space vector pwm control for csi-fed field-oriented induction motor drive with improved performances and reduced pulsating torque. *WSEAS Trans.-Circuits and Systems*, 1(2):71–77, 2005.
- [58] N Muthukumar, Seshadhri Srinivasan, K Ramkumar, K Kannan, and Valentina Emilia Balas. Adaptive model predictive controller for web transport systems. *Acta Polytechnica Hungarica*, 13(3):181–194, 2016.
- [59] László Neukirchner, Attila Gölle, Péter Görbe, and Attila Magyar. Carbon footprint reduction via voltage asymmetry compensation of three-phase low voltage grid utilizing small domestic power plants. *Chemical Engineering Transactions*, 45:283–288, 2015.
- [60] László Neukirchner, Péter Görbe, and Attila Magyar. Examination of different voltage asymmetry norms under transient behavior of three-phase low voltage power systems containing small domestic power plants. In *PowerTech, 2015 IEEE Eindhoven*, pages 1–6. IEEE, 2015.
- [61] László Neukirchner, Péter Görbe, and Attila Magyar. Voltage unbalance reduction in the domestic distribution area using asymmetric inverters. *Journal of cleaner production*, 142:1710–1720, 2017.
- [62] László Neukirchner, Nimród Kutasi, András Kelemen, Attila Fodor, and Attila Magyar. Constrained predictive control of three-phase buck rectifiers simulation details. In <http://virt.uni-pannon.hu/ver/index.php/en/projects/30-empc-csr>. University of Pannonia, 2019.
- [63] Nayeem Ahmed Ninad and Luiz Lopes. Per-phase vector control strategy for a four-leg voltage source inverter operating with highly unbalanced loads in stand-alone hybrid systems. *International Journal of Electrical Power & Energy Systems*, 55:449–459, 2014.
- [64] Thomas Nussbaumer, Martina Baumann, and Johann W Kolar. Comprehensive design of a three-phase three-switch buck-type pwm rectifier. *IEEE Transactions on Power Electronics*, 22(2):551–562, 2007.

- [65] MJ Ortega, JC Hernández, and OG García. Measurement and assessment of power quality characteristics for photovoltaic systems: harmonics, flicker, unbalance, and slow voltage variations. *Electric Power Systems Research*, 96:23–35, 2013.
- [66] Sushree Sangita Patnaik and Anup Kumar Panda. Three-level h-bridge and three h-bridges-based three-phase four-wire shunt active power filter topologies for high voltage applications. *International Journal of Electrical Power & Energy Systems*, 51:298–306, 2013.
- [67] L Pierrat and JP Meyer. Unbalance factor it is as simple as abc. *Revue Générale de l'Électricité*, 1(6):18–26, 1987.
- [68] P Pillay and M Manyage. Definitions of voltage unbalance. *IEEE Power Engineering Review*, 21(5):50–51, 2001.
- [69] Chiheb Ben Regaya, Abderrahmen Zaafour, and Abdelkader Chaari. A new sliding mode speed observer of electric motor drive based on fuzzy-logic. *Acta Polytechnica Hungarica*, 11(3):219–232, 2014.
- [70] M Rivera, S Kouro, J Rodriguez, B Wu, V Yaramasu, J Espinoza, and P Melila. Predictive current control in a current source inverter operating with low switching frequency. In *4th International Conference on Power Engineering, Energy and Electrical Drives*, pages 334–339. IEEE, 2013.
- [71] A Robert and J Marquet. Assessing voltage quality with relation to harmonics, flicker and unbalance. In *International Conference on Large High Voltage Electric Systems*, volume 2, pages 36–203, 1992.
- [72] J Anthony Rossiter. *Model-based predictive control: a practical approach*. CRC press, 2017.
- [73] Rafik Salloum, Bijan Moaveni, and Mohammad Reza Arvan. Robust pid controller design for a real electromechanical actuator. *Acta Polytechnica Hungarica*, 11(5):125–144, 2014.
- [74] Mika Salo. A three-switch current-source pwm rectifier with active filter function. In *2005 IEEE 36th Power Electronics Specialists Conference*, pages 2230–2236. IEEE, 2005.
- [75] Yukihiko Sato and Teruo Kataoka. State feedback control of current-type pwm ac-to-dc converters. *IEEE transactions on industry applications*, 29(6):1090–1097, 1993.
- [76] Mehdi Savaghebi, Alireza Jalilian, Juan C Vasquez, and Josep M Guerrero. Secondary control scheme for voltage unbalance compensation in an islanded droop-controlled microgrid. *IEEE Transactions on Smart Grid*, 3(2):797–807, 2012.

- [77] Lip Huat Saw, Yonghuang Ye, and Andrew AO Tay. Integration issues of lithium-ion battery into electric vehicles battery pack. *Journal of Cleaner Production*, 113:1032–1045, 2016.
- [78] S Segui-Chilet, FJ Gimeno-Sales, S Orts, G Garcera, E Figueres, M Alcaniz, and R Masot. Approach to unbalance power active compensation under linear load unbalances and fundamental voltage asymmetries. *International Journal of Electrical Power & Energy Systems*, 29(7):526–539, 2007.
- [79] SK A Shezan, S Julai, MA Kibria, KR Ullah, R Saidur, WT Chong, and RK Akikur. Performance analysis of an off-grid wind-pv (photovoltaic)-diesel-battery hybrid energy system feasible for remote areas. *Journal of Cleaner Production*, 125:121–132, 2016.
- [80] Arfat Siddique, GS Yadava, and Bhim Singh. Effects of voltage unbalance on induction motors. In *Conference Record of the 2004 IEEE International Symposium on Electrical Insulation*, pages 26–29. IEEE, 2004.
- [81] Asheesh K Singh, GK Singh, and R Mitra. Some observations on definitions of voltage unbalance. In *2007 39th North American Power Symposium*, pages 473–479. IEEE, 2007.
- [82] Károly Széll and Péter Korondi. Mathematical basis of sliding mode control of an uninterruptible power supply. *Acta Polytechnica Hungarica*, 11(03):87–106, 2014.
- [83] Fatima Tahri, Ali Tahri, Ahmed Allali, and Samir Flazi. The digital self-tuning control of step a down dc-dc converter. *Acta Polytechnica Hungarica*, 9(6):49–64, 2012.
- [84] Daniel John Tooth, Stephen Jon Finney, and Barry Wayne Williams. Effects of using dc-side average current-mode control on a three-phase converter with an input filter and distorted supply. *IEE Proceedings-Electric Power Applications*, 147(6):459–468, 2000.
- [85] Antal Ürmös, Zoltán Farkas, Márk Farkas, Tamás Sándor, László T Kóczy, and Ákos Nemcsics. Application of self-organizing maps for technological support of droplet epitaxy. *Acta Polytechnica Hungarica*, 14(4):207–224, 2017.
- [86] Istvan Vajda, Yury N Dementyev, Kirill N Negodin, Nikolay V Kojain, Leonid S Udut, Irina A Chesnokova, et al. Limiting static and dynamic characteristics of an induction motor under frequency vector control. *Acta Polytechnica Hungarica*, 14(6):7–27, 2017.
- [87] Vishal Vekhande, VK Kanakesh, and Baylon G Fernandes. Control of three-phase bidirectional current-source converter to inject balanced three-phase currents under unbalanced grid voltage condition. *IEEE Transactions on power electronics*, 31(9):6719–6737, 2015.

- [88] Thiyagarajan Venkatraman and Somasundaram Periasamy. Multilevel inverter topology with modified pulse width modulation and reduced switch count. *Acta Polytechnica Hungarica*, 15(2), 2018.
- [89] Sasa Vrkalovic, Elena-Cristina Lunca, and Ioan-Daniel Borlea. Model-free sliding mode and fuzzy controllers for reverse osmosis desalination plants. *Int. J. Artif. Intell.*, 16(2):208–222, 2018.
- [90] Xiongfei Wang, Yun Wei Li, Frede Blaabjerg, and Poh Chiang Loh. Virtual-impedance-based control for voltage-source and current-source converters. *IEEE Transactions on Power Electronics*, 30(12):7019–7037, 2014.
- [91] Yaw-Juen Wang. An analytical study on steady-state performance of an induction motor connected to unbalanced three-phase voltage. In *2000 IEEE Power Engineering Society Winter Meeting. Conference Proceedings (Cat. No. 00CH37077)*, volume 1, pages 159–164. IEEE, 2000.
- [92] Yaw-Juen Wang. Analysis of effects of three-phase voltage unbalance on induction motors with emphasis on the angle of the complex voltage unbalance factor. *IEEE Transactions on energy conversion*, 16(3):270–275, 2001.
- [93] Zheng Wang, Bin Wu, Dewei Xu, Ming Cheng, and Liang Xu. Dc-link current ripple mitigation for current-source grid-connected converters under unbalanced grid conditions. *IEEE Transactions on Industrial Electronics*, 63(8):4967–4977, 2016.
- [94] He Wen, Da Cheng, Zhaosheng Teng, Siyu Guo, and Fuhai Li. Approximate algorithm for fast calculating voltage unbalance factor of three-phase power system. *IEEE Transactions on Industrial Informatics*, 10(3):1799–1805, 2014.
- [95] Yan Xu, Leon M Tolbert, John D Kueck, and Dwight T Rizy. Voltage and current unbalance compensation using a static var compensator. *IET Power Electronics*, 3(6):977–988, 2010.
- [96] Zhaoyang Yan, Xiaomeng Xu, Zhenxing Yang, Xiaoyu Wu, and Yuepeng Wang. Study of effective vector synthesis sequence for three-phase current rectifier. In *2015 Fifth International Conference on Instrumentation and Measurement, Computer, Communication and Control (IMCCC)*, pages 1065–1070. IEEE, 2015.
- [97] NR Zargari and G Joos. A current-controlled current source type unity power factor pwm rectifier. In *Conference Record of the 1993 IEEE Industry Applications Conference Twenty-Eighth IAS Annual Meeting*, pages 793–799. IEEE, 1993.